High-resolution modelling of ice and mixed-phase clouds: the GCSS WG2/WG3 experience

Philip R.A.Brown, Ruei-Fong Lin, David O'C Starr and Peter Clark

Met Office, Bracknell, England

1. Introduction

The strategy of the GEWEX Cloud System Study (GCSS) is founded upon the use of cloud-system models (CSMs). These are "process" models with sufficient spatial and temporal resolution to represent individual cloud elements (hence the alternative description as Cloud-Resolving Model, CRM), but spanning a wide range of space and time scales to enable statistical analysis of simulated cloud systems. GCSS also employs single-column versions of the parametric cloud models (SCMs) used in GCMs.

Central to the GCSS strategy is the conduct of model comparison projects. These systematic comparisons document the performance of state-of-the-art models, detect problems with specific models, and identify fundamental issues resulting in significant inter-model differences, such as the approach to representing a specific process. Comparison to field observations, especially in a case study mode, is another cornerstone of the GCSS approach. The concept is that these activities will serve to markedly accelerate community-wide improvements in CSMs, as well as to provide better focus for planned field experiments in terms of key science issues related to the modeling of cloud systems. CSMs are quite well matched, in terms of scales and resolved physical processes, for such comparisons with observations. Moreover, when sufficient confidence is established in the models via validation versus field measurements, CSMs can serve as highly useful research platforms for the development of concepts and approaches to cloud parameterization because they do resolve the physical processes operating in cloud systems to a much greater extent than SCMs. While some processes must still be parameterized in CSMs, such parameterizations are more focused, in terms of the represented physical process, and better correspond to the scales at which such processes actually operate.

The recent revision of the GCSS Science Plan (Randall et al., 2000) details the principal aims of each working group. The major science issues being addressed by WG2 (cirrus clouds) are:

1. What level of microphysical complexity/sophistication is required for adequate treatment of cirrus clouds and their effects in large-scale models (climate and NWP)? A related critical question is: What level of microphysical complexity/sophistication is required for adequate treatment of cirrus clouds in remote sensing applications, both space-based and surface-based? In this respect, how important are the effects of microphysical heterogeneity in the vertical and horizontal dimensions, and how can the absorptance of solar energy be calculated?

2. What vertical resolution is required in large-scale models to enable adequate representation of the large-scale forcing to cirrus cloud formation?

3. To what extent is the parameterization (representation) of cloud dynamical processes and feedbacks (radiation - latent heat - dynamics) required for the treatment of cirrus clouds in large-scale models?

Similarly, to what extent must the ambient mesoscale (gravity) wave environment be explicitly taken into account?

4. What are the effects of the ambient aerosol population on cirrus cloud properties, and do variations in aerosols (or aerosol activation spectra via dynamics) lead to significant variations in cloud properties? How important is heterogeneous nucleation, and when is it important?

5. Can/should the same parametric treatment of cirrus clouds formed via large-scale ascent in a large-scale model be applied to the treatment of the evolution of cirrus formed via detrainment from simulated deep convective cloud systems?

WG3 (Extratropical layer clouds) addresses the following major science questions:

1. How important is it for AGCMs to realistically parameterize sub-grid scale mesoscale cloud structure and cloud layering in extra-tropical cloud systems?

2. What level of complexity of parameterized microphysical processes is needed in order that weather and climate general circulation models can realistically simulate extra-tropical cloud systems?

3. What is the validity of microphysical parameterizations in weather and climate general circulation models for mid-latitude cloud systems forced by orography?

4. Why are climate models deficient in developing clouds in the weakly forced regimes of mid-latitude cloud systems?

5. Why are the components of the water budget associated with mid-latitude cloud systems poorly represented in climate simulations?

The two groups have, therefore, a number of common interests, in particular those relating to microphysical processes. The present work will concentrate on this issue. A number of state-of-the-art general circulation models (GCM) and operational numerical weather prediction (NWP) models now some form of prognostic representation of ice cloud. The potential value of this has been illustrated by number of studies. Gregory and Morris (1995) illustrated the sensitivity of climate simulations using the Met Office GCM to the choice of temperature regime over which mixed-phase cloud was diagnosed. With a prognostic ice variable added to this model (Wilson and Ballard 1999), NWP simulations have improved representation of supercooled stratocumulus cloud, improved representation of freezing rain and supercooled liquid cloud and increased high-altitude ice-cloud amounts. In climate simulations (Wilson 2000), there is improved vertical structure in the vertical profiles of liquid and ice cloud condensate and some reduction in tropical convective activity due to the latent heating from increased ice cloud water.

In the Colorado State University GCM, the addition of prognostic ice cloud (Fowler et al. 1996) lead to improvements in the geographical distribution of cloudiness by comparison with observations from the International Satellite Cloud Climatology Program (ISCCP). There were also improvements in the top-of-atmosphere (TOA) radiation budget and long-wave (LW) and short-wave (SW) cloud forcing. The amount and optical thickness of upper tropospheric clouds was decreased, this effect being largest in tropical regions, and the changes in the distribution of latent heating gave improvements in the model general circulation by comparison with ECMWF analyses. It was, however, noted that simulations using the prognostic ice had important sensitivities to the specification of ice particle fallspeed and to certain key parameters in the

microphysics scheme such as the threshold water content for the onset of autoconversion of cloud ice (non-precipitating) to snow.

Section 2 will examine the comparison of parcel models using explicit liquid and ice phase microphysics in simulations of the initiation of ice under typical cirrus conditions. Section 3 describes the intercomparison of Cloud-Resolving Model (CRM) simulations of the evolution of cirrus in response to simple forcing. Section 4 gives a brief description of some uses of in-situ and radar measurements to validate ice hydrometeor distributions in model simulations.

2. Cirrus Parcel Model Comparison (CPMC)

A number of the CRMs participating in GCSS WG2 incorporate a fully-explicit (multiple size-bin) treatment of the ice-phase microphysical processes. These represent both homogeneous and heterogeneous nucleation processes. Closed-parcel models with explicit microphysics have been used in a number of studies to examine the cirrus formation process. Sassen and Dodd (1988) compared model results with lidar observations of cirrus, so as to infer the homogeneous nucleation rate of supercooled cloud droplets. Heymsfield and Sabin (1989) examined the homogeneous freezing of droplets and haze particles formed on ammonium sulphate aerosol. Parameterizations of the homogeneous freezing process for regional scale models were developed by DeMott et al. (1994). Jensen et al. (1998) and Lin et al. (1998) compared parcel model simulations with observations from orographic clouds. Such studies have provided some insight into the dependence of the freezing process on CCN number concentration and chemical properties and also on the potential impact of heterogeneous ice-forming nuclei (IN) (Sassen and Benson 2000, Spice et al. 1999). One key element missing from these studies has been an estimate of the quantitative uncertainty in such parcel model predictions of cirrus microphysical properties, so estimates of the magnitude and source of these uncertainties were one of the principal foci of this project.

The CPMC specified a number of relatively simple simulation scenarios, with a closed parcel lifted at a fixed updraught velocity without exchange of heat or mass with its environment. The main interest was in the homogeneous freezing process operating alone (HN-ONLY) although simulations were also conducted using each model's methods of representing the action of heterogeneous IN (ALL-MODE).

2.1 Simulation details

Two different temperature regimes were specified, so as to simulate the nucleation conditions occurring in the "Warm" and "Cold" cases of the Idealized Cirrus Model Comparison (ICMS: see below). These correspond roughly to cloud top temperatures of -42 and -63 C, respectively. All the models describe closed Lagrangian parcels, so that no particle fallout or mixing with the environment was allowed. Fixed updraught velocities of 0.04, 0.2 and 1.0 ms^{-1} the former being characteristic of synoptic scale events whilst the latter is more representative of the updraughts encountered in mountain lee-wave or turbulent mid-latitude cirrus. An aerosol size spectrum is specified with a total concentration of 200 cm^{-3} and a log-normal distribution with mode radius 0.02 μm and width, σ=2.3. The aerosol particles are composed of sulphuric acid. All ice crystals nucleated were assumed to be spherical with a bulk density equal to that of solid ice, 0.9 g cm^{-3}. The impact of aggregation and the radiative heating of particles were both ignored. The amount of vertical lifting was set sufficiently large to ensure that all models made a complete transition through the nucleation regime to a state of approximate equilibrium between the depositional growth of the ice and the condensation rate generated by the updraught.

2.2 Model details

Brief details of the models participating in the study are given in Table 1. These will subsequently be referred to as models C, D, J, K, L1, L2, and S. Model S is a particle-tracing model in which the evolution of a large number of individual particles is followed during the simulation. The other models distribute particles into a number of different size classes (size-bins). From the microphysical point of view, the major components of each model are its treatment of the saturation vapour pressure, the diffusional growth of haze particles and ice crystals, the equilibrium size and solution concentration of haze particles, and the homogenous and heterogeneous nucleation schemes. The CPMC concentrates on the latter three.

Organization **Investigator**	**UKMO** **Cotton**	**CSU** **DeMott**	**ARC** **Jensen**	**DRL** **Kaercher**	**GSFC** **Lin**	**U Mich** **Liu**	**U Utah** **Sassen**
Time Step	0.01	10/W(W in cm/s)	Adjusting10^{-5} to 0.02	fixed	0.02	0.02	0.01
Bin	Discrete	Continuous	Continuous	Moving Center	Continuous	Particle Tracing	Particle Tracing
Haze Particle Size	DIFF	EQ	EQ	DIFF	DIFF/EQ	DIFF	DIFF
Heterogeneous Nucleation	Si Dependent	Immersion Freezing	Not Submitted	Not Submitted	Si Dependent	Not Submitted	Modified Fletcher
Homogeneous Nucleation	Teff	Teff	Modified classical	Koop et al (2000)	Teff	Teff	Teff
Γ	1.5	1.5	Varying*	Varying*	1.0	2.0	1.7
B_i	0.24	0.04	1.0	0.5	0.1	0.1	0.36

Table 1 Details of models participating in Cirrus Parcel Model Comparison

DIFF: diffusional growth
EQ: equilibrium size
Teff: effective freezing temperature approach
$T_{eff}=T+\lambda\Delta T_m$
B_i: deposition coefficient

2.3 Homogeneous nucleation rate of haze particles

A number of recent studies (eg. Sassen and Dodd 1988, DeMott and Rogers 1990, Pruppacher 1995, Jeffery and Austin 1997) involving both theory and observations have lead to a developing concensus concerning the homogeneous nucleation rate of ice in pure water, J_W. This does, however remain an active research area, and is of great importance in the formation of cirrus cloud since all studies show that J_W varies by around one order of magnitude per degree at temperatures of around -45 C.

Model J determines the haze particle nucleation rate, J_{haze}, from the modified classical theory (Pruppacher and Klett 1997). This depends on values of the surface energy of the ice-solution interface, the activation energy, and the ice germ formation energy. Model J relies on observations of the ice-solution surface energy and uses observations of J_{haze} to detemine the activation energy, following Tabazedeh et al. (2000).

The other models rely on the so-called "effective temperature" approach. This attempts to link measured nucleation rates of solution droplets to those of equivalent-sized pure water droplets by means of the effective freezing temperature, T_{eff}, which is defined following Sassen and Dodd (1988) by

$$J_{haze}(T) = J_W(T_{eff}) \tag{1}$$

with

$$T_{eff} = T + \lambda \Delta T_m \tag{2}$$

where ΔT_m is the equilibrium melting point depression of the solution, dependent on its concentration and λ is an empirical constant to account for the additional impact on nucleation of non-ideal interactions between solute ions and water molecules. Since the calculated nucleation rate is highly-sensitive to the choice of ΔT_m and λ, these two parameters must be specified with care. Values of λ are constrained by laboratory data, as described by Sassen and Dodd (1988), who noted an average value of 1.7. However, the value for specific solutions may vary between 1 and 2.5 (DeMott 2001).

The nucleation rates computed by the modified classical theory used by model J and the effective temperature approach of the other models are shown in Figure 1. All models use a standard set of equilibrium haze particle data. Models C, D, L and S all use λ=2 and fitted values of from DeMott et al. (1997). Curves for these four models differ due to the different functional representations of J_W. Their sensitivity to the solute concentration is much greater than that of model J, and the consequences of this are considered below. Differences in the value of λ affected the critical relative humidity at which nucleation commences. If this were the only variable parameter, then it would be expected that nucleation would occur first in the model with the lowest value since haze particles freeze at a higher solute concentration and hence at a lower RH_W. Therefore, the range of solute concentration corresponding to a given $\lambda \Delta T_m$ may be used to estimate to first order the triggering RH_W. It can be shown that this solute concentration range increases with $\lambda \Delta T_m$ whilst the required value of $\lambda \Delta T_m$ to trigger nucleation increases with decreasing temperature. We may then conclude that the triggering RH_W for nucleation becomes more sensitive to λ as temperature decreases, and this will be further demonstrated in the model results.

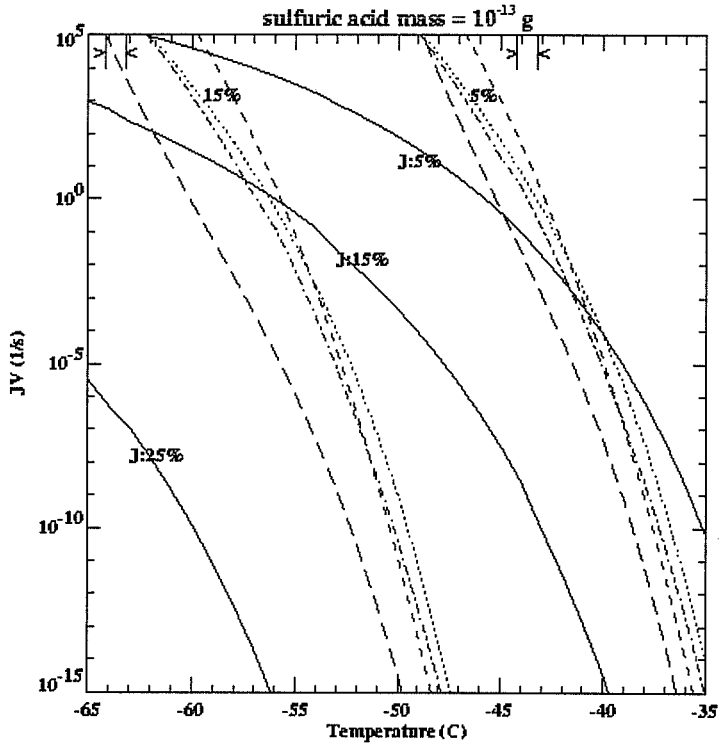

Figure 1: Homogeneous nucleation rate times equilibrium haze particle volume, $J_{haze}V$, as a function of temperature for particles with a sulphuric acid mass of 10^{-13} g, when the solute concentration by weight is 5, 15 and 25%. Solid lines are for model J which uses the classical nucleation theory, whilst the other curves are for models using the effective temperature approach.

2.4 Heterogeneous nucleation

There is still a lack of both theoretical and experimental understanding of heterogeneous ice nucleation processes in the atmosphere so no constraints were applied to individual models. Two parameterizations dependent only on the ice saturation ratio were used.

$$N_{IN} = 2.7.10^{10}(S_I - 1)^{\beta} \tag{3}$$

from Spice et al. (1999) was used by model C, whilst

$$N_{IN} = \exp[7.5468 + 12.96(S_I - 1)] \tag{4}$$

from Meyers al. (1992) was used by model L.

At high values of S_I, the values of N_{IN} given by these two expressions may exceed the range of values 0.1 to 100 litre^{-1} reported from aircraft measurements by Rogers et al. (1998). The majority of these data were obtained between 15 and -40 C and between ice saturation and about 15% water supersaturation. Since IN activation depends on temperature and humidity, it is possible that more IN are active at lower temperatures than in the Rogers et al. measurements. Nevertheless, the two expressions above are expected to give a reasonable estimate of the maximum impact of heterogeneous nucleation.

Models D and S treat heterogeneous nucleation explicitly. Model D assumes that 10% of the sulphuric acid CCN larger than 0.1 μm contain 50% insoluble matter with a bulk density of 1.9 g cm^{-3} as deduced from observations at temperatures down to -35 C by DeMott et al. (1998). The average freezing nucleus spectrum from that study was extrapolated to the temperature range of the CPMC. Thus the fraction of IN in each haze size class, k (>0.1 μm), was given by

$$F_k = \frac{1.3.10^{23}}{F_{(>0.1\mu m)}}(273.15 - T_{eff,k})^{11.75} \tag{5}$$

where $F_{(>0.1\mu m)}$ is the fraction of CCN larger than 0.1 μm compared to the total CCN. This expression is expected to give the smallest impact of heterogeneous nucleation in the CPMC study.

Model S assumes that heterogenous IN activation follows the form given by Khvorostyanov and Sassen (1998a),

$$\frac{dN_I}{dt} = \sum_k A_{S0} B_S \exp(-A_Z z) \exp[B_S(273.15 - T_{eff,k})] \frac{dT}{dt} \tag{6}$$

with $A_{S0}=0.1$, $B_S=0.8\ K^{-1}$ and $A_Z=7.5.10^{-4}\ m^{-1}$. This is a modified form of the well-known Fletcher expression with a height-dependent term. A higher than typical value of B_S is used so as to allow heterogeneous nucleation to compete more strongly. Model S traces a total of 20000 particles so that its minimum detectable change in ice number concentration is around 0.01 cm^{-1}.

2.5 Simulation results

Figure 2 illustrates the evolution of each of the models for the "Cold" simulation with $w=0.2$ ms^{-1}. Four separate stages may be identified. In the first stage, the ascending parcel cools adiabatically and haze particles grow, although there is negligible uptake of water vapour.

The second (nucleation) stage begins as the first crystals form. The cirrus cloudbase, z_b, is arbitrarily defined as the level at which N_I reaches 1 litre^{-1}. IWC and N_I increase thereafter and the tendency of RH_I remains positive but decreasing in magnitude to the vapour uptake by growing crystals. Homogeneous nucleation, when active, ceases shortly after RH_I reaches its peak value, so that all nucleation occurs within a small range of vertical displacement of the air parcel.

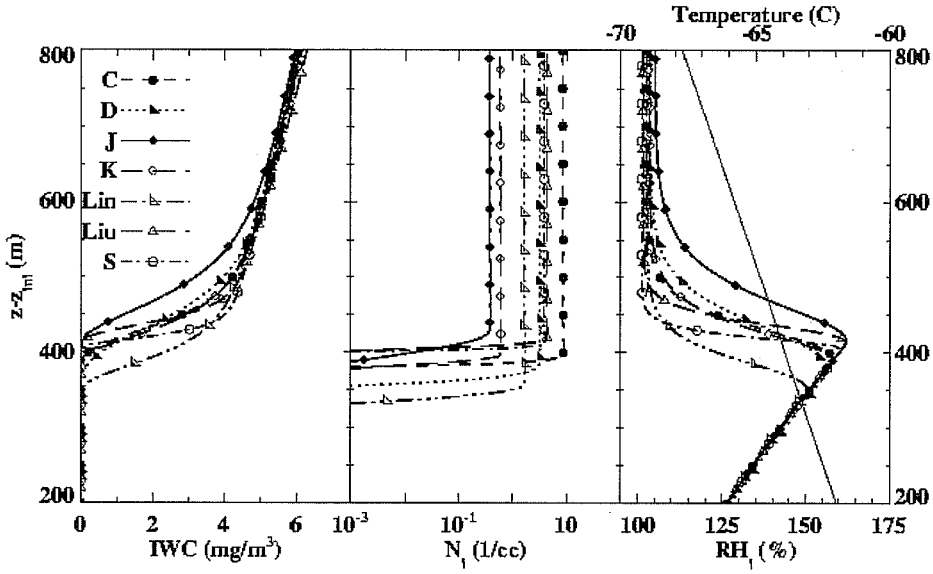

Figure 2. The variation of IWC (left), number concentration N_I (centre) and relative humidity w.r.t. ice (right) for simulations of the CPMC Cold case at an updraught velocity of 0.2 ms^{-1}.

In the third stage, RH_I declines rapidly corresponding to the increase of IWC. The final quasi-equilibrium stage begins when the RH_I tendency approaches zero, when any further vapour excess produced by lifting and cooling of the parcel is taken up by ice crystal growth.

Figure 3 compares values of ice number concentration, N_I, after 800m of ascent. For HN-ONLY cases, then to a first approximation $log(N_I)$ increases linearly with $log(w)$. This relationship was also demonstrated by Heymsfield and Sabin (1989) and Sassen and Dodd (1988) and others. Whilst all models in the present study exhibit the same qualitative behaviour, there is a factor of up to 25 difference between them and the reasons for this difference will be examined. Comparing the two temperature regimes, more ice crystals are generally produced in the cold simulations. Jensen and Toon (1994) hypothesized that this is due to the reduced ice crystal growth rates at lower temperatures.

The range of cloudbase RH_I is smaller in warm cases than in the cold. In the models which describe homogeneous nucleation using the effective temperature, T_{eff}, the range of critical freezing RH_I corresponding to a given range of λ increases with decreasing temperature. Generally, smaller λ gives a lower cloudbase height. However, the cloudbase RH_I is also dependent on other factors such as solution density and the specifications of haze particle solute concentration and saturation vapour pressure over water. Thus, for the cold case models C and D, both using λ=1.5 obtain different values for cloudbase RH_I, and in the warm cases the sequence of the times at which nucleation is triggered does not follow the sequence of values of λ.

For the ALL-MODE simulations, the cloudbase altitude, z_b, and relative humidity, RH_I, vary even more widely, due to the different methods of heterogeneous nucleation. The impact on N_I, peak RH_I, and cloud

formation altitude is extremely sensitive to the onset conditions for nucleation and the subsequent ice crystal growth. With heterogeneous nucleation activated, the peak RH_I and maximum N_I are reduced in almost all cases. We may define an N_I reduction ratio as N_I for an ALL-MODE case divided by the corresponding value for HN-ONLY. Values are shown in Table 3. The relatively small values for models C and L are directly due to their heterogeneous nucleation schemes which are only dependent on S_I and not affected by any link to aerosol number concentration or size and also the low RH_I onset conditions for heterogeneous nucleation {eg. $S_I > 1$ for model L). In model D, which is expected to have the least impact of heterogeneous nucleation (see above), IN only have an impact for the warm, slow updraught case (w = 0.04 ms^{-1}). This weak influence is related to two factors. Firstly, the maximum IN concentrations predicted by the formulation are no more than a few hundred per litre in the range of conditions that are simulated. Secondly, the lowering of the onset RH_I for ice formation is limited by solute concentration via the use of effective freezing temperature in the immersion freezing mechanism.

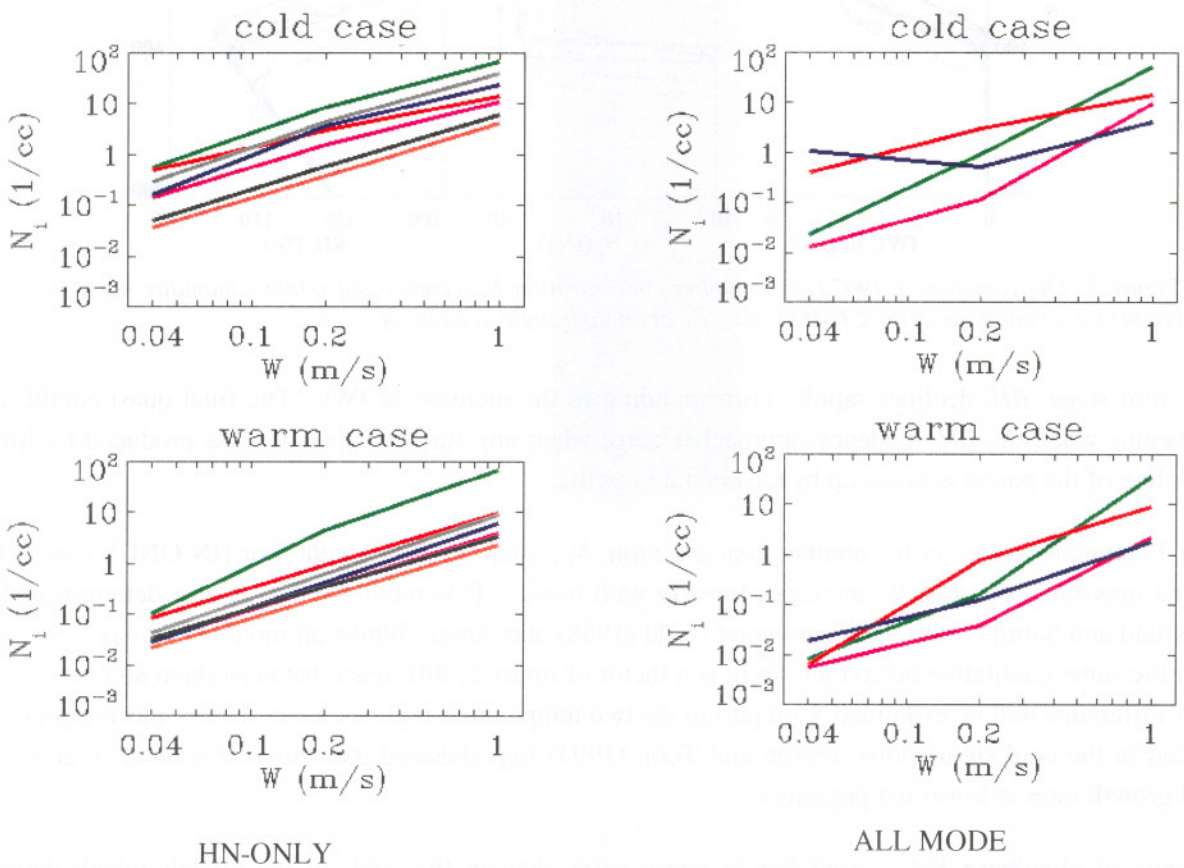

Figure 3: Ice number concentration, NI, as a function of updraught velocity, w. Cases with homogeneous freezing only (HN-ONLY) are in the left column, those with heterogeneous nucleation acitivated (ALL_MODE) in the right.

The N_I reduction ratios for model S are significantly higher for updraughts of 0.04 ms^{-1}. Indeed at this velocity, N_I is higher for ALL-MODE than HN-ONLY. It is possible that this behaviour results from the large value of B_S used in its expression for heterogeneous nucleation (6). However, this large value is necessary to generate a significant number of heterogeneously-nucleated crystals, due to the height dependent term. This indicates a clear need for further measurements to understand the temporal and spatial distribution of heterogeneous IN.

2.6 Causes of variability in simulations with fixed λ

A number of factors interact with each other in generating differences in crystal number concentration in HN-ONLY runs. For a given temperature, size and solute concentration of a haze particle, differences in formulating the homogeneous nucleation rate alter the freezing probability of a single particle. For a given updraught velocity, the diffusional growth rate of ice crystals controls the uptake of water vapour, the evolution of the parcel RH_W, and hence the final predicted N_I. Results from simulations with fixed λ (=2.0) are now examined in order to examine these interactions in depth. Using a fixed value of this parameter in all simulations is an attempt to minimize differences in nucleation rates between the different models. Model J attempted as far as possible to match the nucleation rates predicted using λ=2 in the effective temperature-based models.

It was found that the nucleation regimes of all models occurred within a 1 K range in both cold and warm cases. Since the effect of this small temperature variation on nucleation rate is secondary compared to the evolution of RH_W, then it is reasonable to analyze the model results by reference to height above cloudbase, $(z - z_b)$. Results of this analysis are shown in Figure 4. As expected, the range of triggering RH_W was reduced to less than 2% and 5% in warm and cold cases, respectively, compared to 3% and 8% for the standard runs at the same vertical velocity. It should be noted that each model uses different expressions to determine the saturation vapour pressure over water and ice. These expressions begin to diverge at temperatures below -45C so the present results are expressed in terms of. RH_W

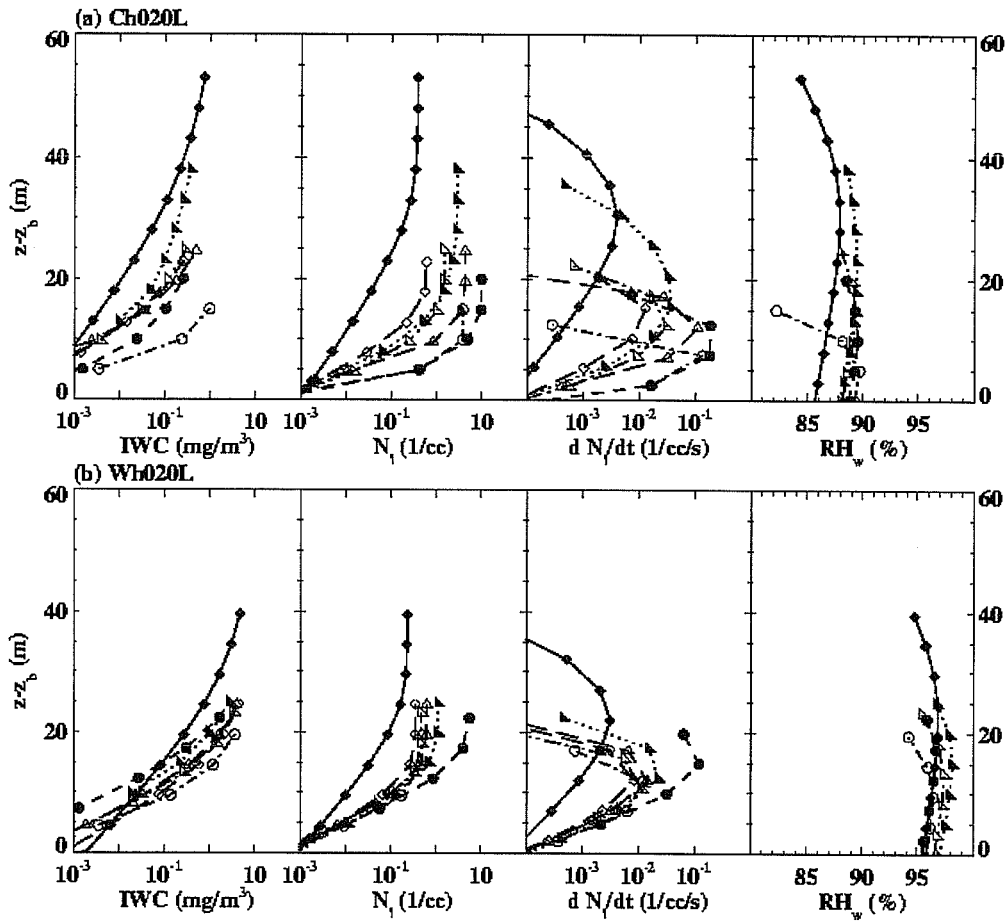

Figure 4: The variation with height above cloudbase of (from left to right) IWC, number concentration, N_I, nucleation rate, d N_I/dt, and relative humidity, for simulations with an updraught velocity of 0.2 ms^{-1}. Upper row (a) shows Cold cases whilst lower row (b) shows Warm cases.

With $\lambda = 2.0$, there are still significant differences in N_I and the individual model results only differ by small amounts from the control runs. It is clear, therefore, that λ is not the dominant factor controlling N_I.

At the start of the nucleation stage in the warm case with $w = 0.2$ ms^{-1} (Wh020L), ice nucleation rates are very similar in the four models of the effective temperature group (Figure 4). However, models C and D reach much higher RH_W leading to higher instantaneous nucleation rates sustained for a longer period than models L and S. Models C and D thus generate the highest N_I. In the corresponding cold case, Ch020L, the grouping of models is slightly different. From the start of the nucleation stage, models D and L are distinctly separate from C and S. Haze particles are in equilibrium in models D and L whilst large haze particles are more concentrated than the corresponding equilibrium value in models C and S. The ice formation rates in C and S are more than an order of magnitude larger than in D and L. However, the nucleation regime is not sustained for as long in model S compare to C. There is a similar comparison between models D and L. Near the end of the nucleation stage, model C has the highest N_I . Model S has only a slightly larger value than model D, despite the fact that the former has a much higher initial ice formation rate. The long duration of nucleation in model D results in a final N_I comparable to model S.

The ice formation rate of model J is smaller than for the effective temperature group of models, and it also has wider range of RH_W between cloudbase and the peak altitude. This model has a much broader number distribution of the haze particles that are actually frozen. These three features are thought to result from a combination of effects. The homogeneous freezing scheme of model J is much less sensitive to solute concentration compared to the effective temperature models, and the curvature effect is ignored when calculating haze particel sizes. With an ice formation rate an order of magnitude smaller than the other models and a longer duration of nucleation, the mean crystal size produced by this model at the end of nucleation can be significantly larger than for the other models.

Figure 4 shows that the ice nucleation rate is approximately normally distributed in the vertical. Therefore, the final ice concentration may be approximated as

$$N_I = \sqrt{\pi / 2}\left(\frac{dN_I}{dt}\right)_{\max} \Delta t \qquad (7)$$

where Δt is the duration of nucleation and $(dN_I / dt)_{max}$ the peak nucleation rate. The evolution of IWC, which is the cumulative uptake of vapour by depositional growth, will control the peak RH_W and hence $(dN_I / dt)_{max}$. The growth rate of small ice crystals $(r < 10\ \mu m)$, under the influence of kinetic effects, is quite sensitive to the value of the deposition coefficient, β_I , so sensitivity tests were performed with different values of this parameter to examine its effect in isolation. Models D and L found that by varying β_I across the range of values used in control runs, 0.04 to 1, then a factor of about 5 or 10 variation in N_I can be produced in warm and cold cases, respectively (see Figure 5). Nucleation begins at the same RH_W but simulations with smaller β_I can reach higher RH_W and so trigger the freezing of smaller haze particles. By adjustment of this factor alone, model D was able to reproduce the lower N_I predicted by model J.

The equilibrium relative humidity, $RH_{I,eq}$, of the parcel models (see section 2.5 above) provides GCMs and CRMs that use a moisture adjustment scheme to convert excess water vapour to cloud ice mass (eg. Starr and Cox, 1985; Krueger et al. 1995) with guidelines to set an appropriate threshold value. It can be shown that $RH_{I,eq}$ is proportional to w and inversely related to N_I. $RH_{I,eq}$ remains within 110% except for cases Wa020 and Ca020 for model L1. However, the moisture adjustment timescale (between peak RH_I and $RH_{I,eq}$) has also to be considered. This timescale decreases exponentially with updraught speed; for $w = 0.04, 0.2, 1.0$ ms^{-1} the values are in the ranges 30-100, 6-40 and 1-6 minutes, respectively. Hence, $RH_{I,eq} > 110\%$ can

frequently be detected in regions of weak uplift. GCMs using timesteps of order 1hr may set a nucleation RH_I and a threshold RH_I to simulate cold cirrus in synoptic scale ascent.

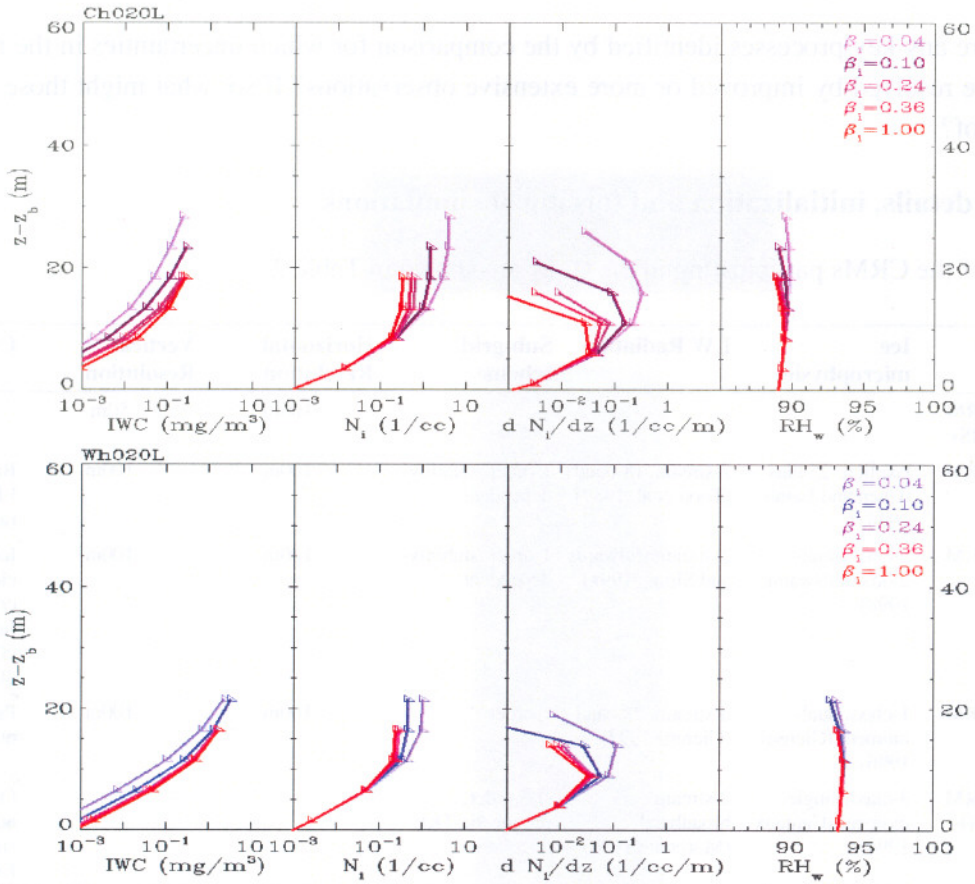

Figure 5: As Figure 4, but results from a single model, L1, with different values of the accommodation coefficient β

3. Idealized Cirrus Model Comparison (ICMC)

The CPMC has tested aspects of explicit microphysics schemes in very simple forcing situations, with no feedback from other processes such as radiative and latent heating or turbulence. The ICMC aims to compare 2- and 3-d CRMs in idealized simulations of cirrus, to provide guidance on the key physical processes and feedbacks acting during the formation, evolution and dissipation of cirrus clouds. A number of SCMs also participated in the project but theses results will not be discussed here. In any attempt, such as this one, to compare a large number of models it is inevitable that some of the information necessary to answer particular aspects of model performance could not readily be made available by certain of the participants. Hence, we cannot attempt to complete a definitive comparison. Nevertheless, we hope to use the information that is available from the various models to address a number of questions:

1 What are the main sources of disagreement between cloud-resolving models? Does the standardization of representation of these key features lead to a greater convergence between models?

2 Are the CRM results capable of providing guidance on the degree of microphysical complication that is necessary or desirable in global models?

3 Can we identify similarities in the cloud structures generated by classes of models which can be described as having similar formulation? When verified against observational data, will the CRMs be capable of describing the sub-grid scale structure in global models?

4 Are there any key processes identified by the comparison for which uncertainties in the model results might be resolved by improved or more extensive observations? If so, what might those observations consist of?

3.1 Model details, initialization and forcing of simulations

Some details of the CRMs participating in the study are shown in Table 2.

Name	Type	Ice microphysics	LW Radiation	Sub-grid scheme	Horizontal Resolution	Vertical Resolution	Comments
BEN (CSU)	3-d CRM (RAMS)				100m	50m	
BHM (PSU)	2-d CRM	Explicit, 25 bins (Chen and Lamb 1994)	2-stream, 18-band (Toon et al. 1989)	1-order, stability dependent	100m	100m	Based on model of LIN, but different radiation scheme.
BRN (Met Office)	3-d CRM	2-class, dual-moment (Swann 1998)	2-stream (Edwards and Slingo 199x)	1-order, stability-dependent.	100m	100m	Ice classes are cloud ice (pristine crystals) and snow (aggregates). Fixed effective radius = 30 micron)
GRN (DLR)	2-d CRM	1-class, dual-moment (Gierens 1996)	6-stream, 28 band (Gierens 1993)	1-order	100m	100m	Prognostic aerosol number density.
GRD (LOA)	2-d CRM (MESO-NH)	3-class, single-moment (Caniaux 1994)	2-stream broadband (Morcrette 1989)	1.5 order, prognostic TKE.			Only pristine ice activated in these simulations. Exponential distribution of particle volume.
JEN (ARC)	2/3-d CRM	Explicit, 25 bins	2-stream (Toon et al. 1989)	1-order, stability-dependent	200m	50m	
KHV (U. UTAH)	2-d CRM	Explicit			200m	200m	
KHL (GFDL)	2-d CRM	2-class, single-moment			100m	100m	Fixed effective radius for ice = 75 micron. 2 classes are cloud ice, snow. Cloud ice non-precipitating
LIN (GSFC_L)	2-d CRM	Explicit, 25 bins (Chen and Lamb 1994)	2-stream, Fu and Liou (1993)	1-order, stability/shear dependent.	100m	100m	
MAR (FRSGC)	3-d CRM (GESIMA)	2-class, single moment	2-stream, Schmetz (1984)		400m	100m	
STR (GSFC_S)	2-d CRM	1-class, single-moment	2-stream broadband, Starr and Cox (1985)		100m	100m	
WTO (GSFC_T)	3-d CRM (GCE)	3-class, dual moment	2-stream, 8-band (Chou and Suarez 1994)		50m	50m	

Table 2 Characteristics of models participating in the WG2 ICMC study

Two basic sets of simulations are defined and referred to as "warm" and "cold" cirrus, the approximate cloud top temperatures being –47C and –66C, respectively. Horizontally uniform profiles of temperature and relative humidity are defined in each case, based on typical conditions for Spring/Fall 45 degN and Summer

30 degN for the warm and cold cases, respectively. These profiles have the common characteristics of a 1km deep layer with a temperature profile that is neutrally-stable with respect to ice-saturated pseudoadiabatic ascent. Within this layer, the initial relative humidity with respect to ice reaches a value of 120% over a depth of 0.5km. The models are forced with an imposed temperature tendency of approximately 1 K hr^{-1} to simulate large scale ascent at 3 cm s^{-1}. This is applied in full over the region 1km below and 1km above the neutrally-stable layer, and decreased linearly to zero over altitude ranges of 1km below and 0.5km above. The initial temperature profile has a region of enhanced stability below the neutrally-stable layer, so that the imposed cooling does not lead to the generation of convective instability during the 4-hour period for which it is applied. After 4 hours, the forcing is switched off and the models allowed to run for a further 2 hours so as to simulate a dissipating cloud layer. The initial potential temperature and relative humidity profiles for the warm case are shown in Figure 6 with the neutrally-stable cloud-forming layer between 8 and 9km. The profiles for the cold case have a similar shape, but with the neutrally-stable layer located between 13 and 14km. Sensitivity tests were run for Warm and Cold cases in which the neutrally-stable layer was replaced by one which was made statically-stable.

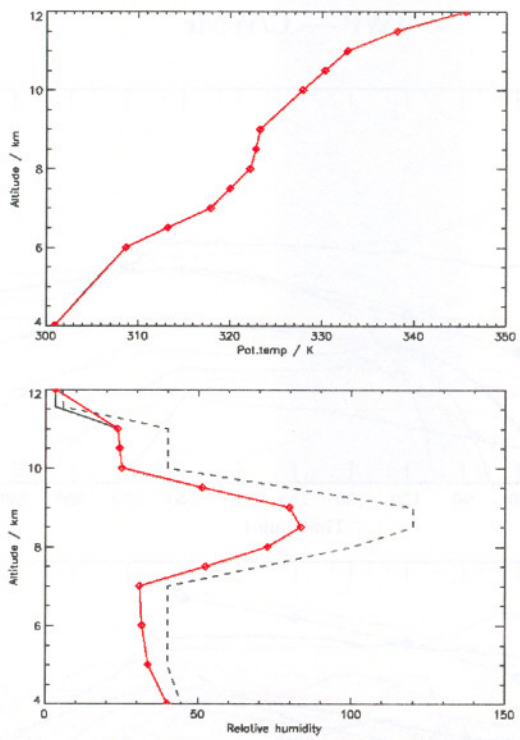

Figure 6: Vertical profiles of potential temperature (upper panel) and relative humidity (lower panel) for initialisation of models in the ICMC comparison Warm cirrus case. The dashed line in the lower panel shows relative humidty w.r.t ice. Profiles were similar for the cold case, but with the moist and neutrally stable layer located between altitudes of 13 and 14km

Within the initial neutrally-stable layer, random temperature perturbations of +/- 0.01K are imposed on the grid scale. Separate tests with one of the models (GSFC_S / Starr) determined that this was a suitably low value, able to initiate motions within the layer but that did not lead to the development of spurious mean horizontal or vertical motions in those models run with open lateral boundary conditions.

All of the models in the study included a fully-interactive radiation scheme capable of describing both long-wave and short-wave radiation. In this project, we chose to use only the long-wave scheme in each model, so as to represent a night-time cloud. This avoids complications due to uncertainties in the representation of the scattering of solar radiation by ice crystals and its dependence on crystal habit, since the latter is not yet prognosed by the microphysical schemes operating in the models. We note, however, that even with the

simplification of using only LW radiation, different models may still be expected to have different treatments of the ice crystal effective radius and hence to produce different relationships between ice water path and optical depth.

A number of the 2- and 3-d CRMs contain a fully-explicit (multiple size-bin) microphysics representation. The specification of aerosol properties in these schemes (on which the initial ice crystal population depends) was taken to be the same as that given in the comparable warm and cold cases of the CPMS, i.e. the aerosol are assumed to be sulphuric acid droplets, in concentrations of 200 cm^{-3}

3.2 Time evolution of integrated ice water path.

Figure 7 shows the evolution with time of the integrated ice water path (IWP) from all simulations. In this figure, the models are not identified individually but the key breaks them down into groups representing SCMs, 2- and 3-d CRMs. The latter are further broken down into those models with an explicit bin-wise microphysics representation and those with various types of bulk-water microphysics schemes.

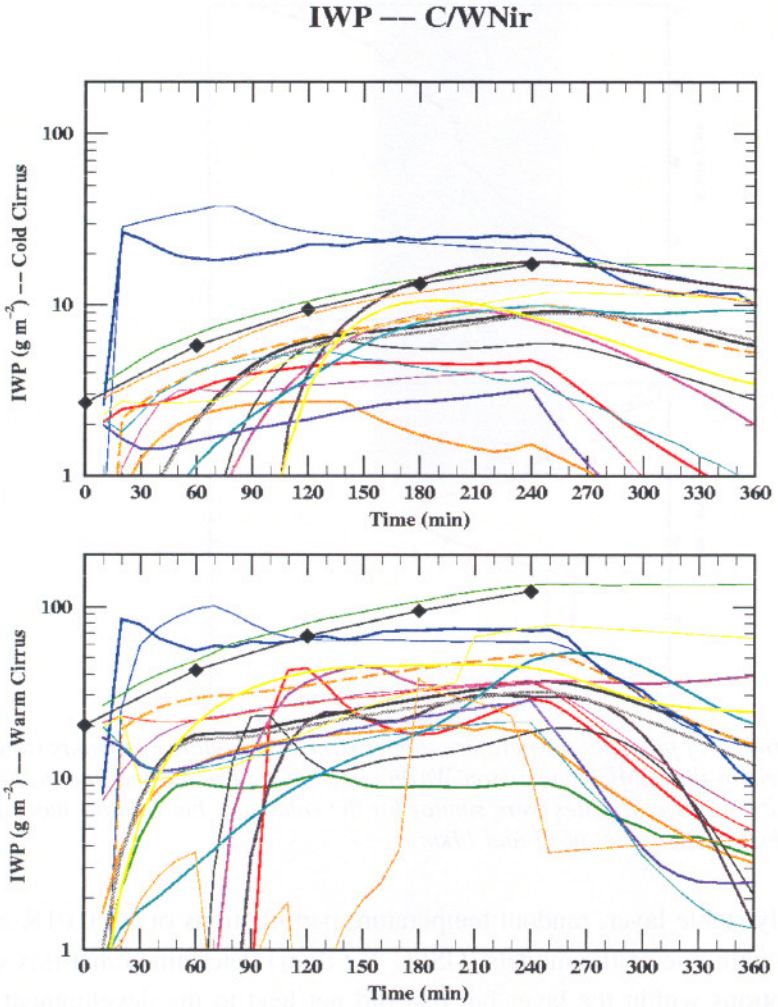

Figure 7: Variation of integrated ice water path, IWP, with time for standard Cold (upper) and Warm (lower) simulations from ICMC. The solid line with symbols indicates the variation with time of the potential IWP that is generated solely by continued cooling of the initial moisture profile (see text for explanation).

It is immediately obvious that there is a large spread of at least an order of magnitude in IWP. Furthermore, there are a number of differences in the time of onset of cloud. The latter may be explained in relatively straightforward terms, by reference to the ice nucleation schemes active in each model. In those models in which ice nucleation occurs by a heterogeneous process, this is commonly dependent on either the ice saturation ratio (Meyers et al. 1992) or temperature (Fletcher 1962). In both cases, the supersaturation in the neutrally-stable layer ensures that cloud forms rapidly, within the first ten minutes of the simulation. Those models with explicit microphysics typically represent nucleation by the homogeneous freezing of aerosol solution droplets. Model (Heymsfield and Sabin 1989) and observational (Heymsfield and Miloshevich 1993) studies of this process show that for temperatures below –38C (ie. within the range of cloud formation temperatures for both warm and cold cases in the present study) nucleation occurs at a critical relative humidity which is dependent on temperature and vertical velocity. For these explicit microphysics models, cloud formation only occurs once the combination of large-scale cooling and the cooling in updraft circulations generated by the perturbation temperature field enables the critical relative humidity to be achieved. Additionally, one of the CRMs with bulk microphysics (Brown) attempts to simulate homogeneous nucleation by only allowing ice nucleation when water saturation is achieved on a grid point. Whilst this is a reasonable approximation for cloud formation temperatures close to –40C, the requirement to achieve water saturation does ensure that this model is the last to form cloud.

A further aspect of the model time evolution behaviour is that some of the models are still spinning-up cloud at 2.5 hours (typically those which implement some form of homogeneous ice nucleation). However, between 3 and 4 hours, the IWP of the majority of models varies only slowly, with the majority showing a slow increase. We therefore take this 3-4 hour period as representative of the models' quasi-equilibrium response to the imposed forcing.

Figure 8 presents vertical profiles of the domain-averaged IWC for each of the models. For convenience, both warm and cold cases appear on the same plot for each model. Examination of these profiles shows that the CRMs can be grouped into one of three different types of behaviour. These will be illustrated below and the terminology used subsequently throughout this paper. The first group have IWC profiles which increase steadily from cloud-top to cloud base and are referred to subsequently as "bottom-peaked". The second (and smaller) group have IWC profiles that have a maximum near the cloud top and are referred to as "top-peaked". The third group have a more obvious two-layer IWC profile and are referred to as such. It should be noted that this division is somewhat arbitrary but is made in order to facilitate subsequent discussions.

If we again examine the IWP time-series shown in Figure 7, we find a group of models that have an initial IWP close to the potential value of 20.2 gm-2 determined above for the start of the simulation. Two of these models, MetOffice and GSFC_T (Brown-het and Wang/Tao) both include a prognostic ice crystal number concentration with ice nucleation being described by a heterogeneous process that is a function only of the ice saturation ratio, following Meyers et al. (1992). Ice can therefore form from the first timestep of the simulation and the initial supersaturation field is removed within the first ten minutes (it may be quicker than this but this is the first time at which we examine model diagnostics). In both cases, however, the number concentration is greater than that specified by the Meyers et al. parametrization

The models PSU and GSFC_L (Boehm and Lin) both include a parametrization of homogeneous nucleation. It has, however, been confirmed that it is not active during their standard warm cirrus simulations and that nucleation is occurring though heterogenous processes, again as parametrized by Meyers et al. (1992). This is in accord with results from the CPMC (Section 2.5 above) which show that heterogeneous nucleation

tends to dominate over homogeneous in simulations in which both processes are allowed. Ice nucleation occurs rapidly at the start of the simulation, ice number concentrations reaching their maximum value within

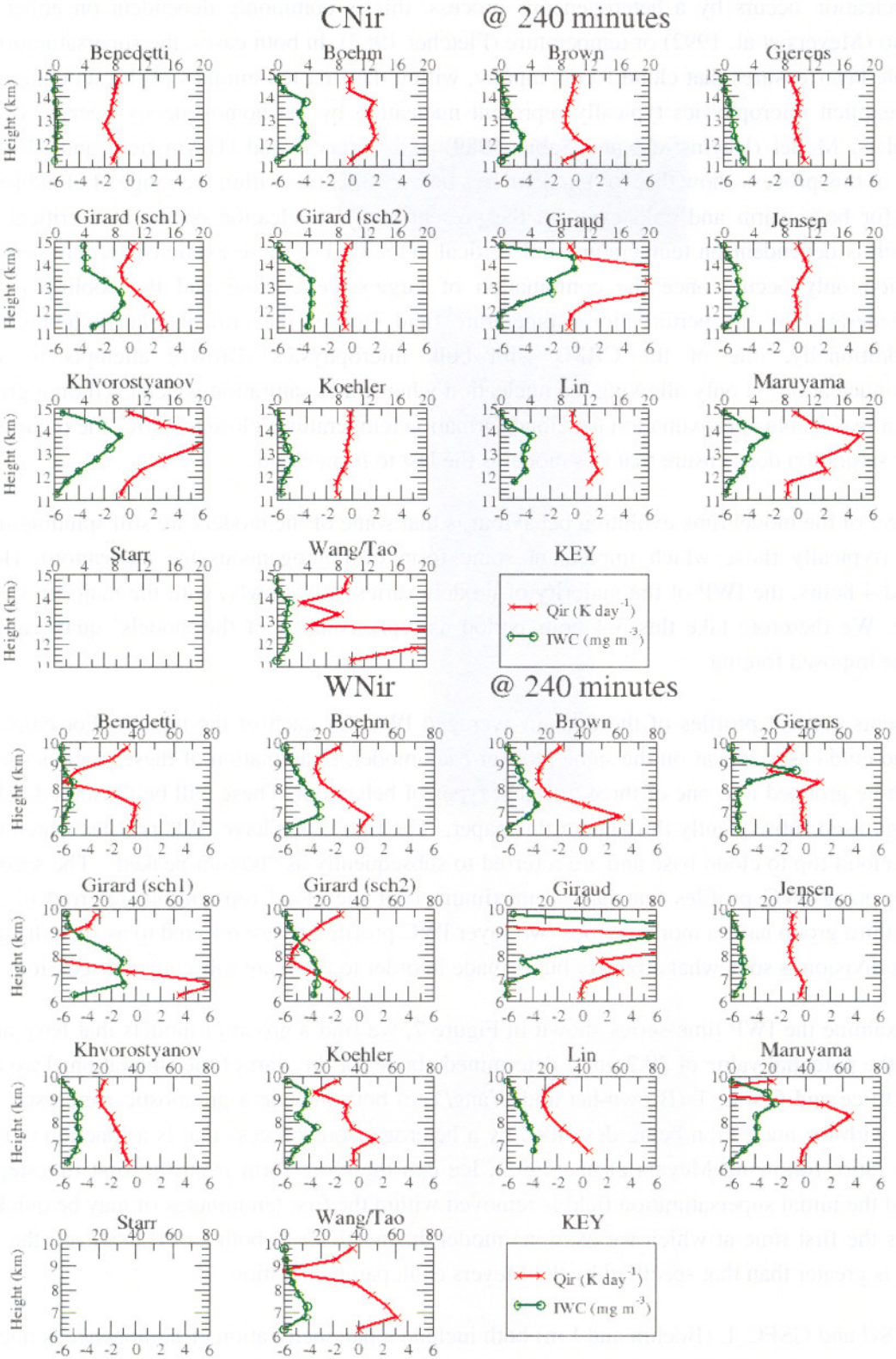

Figure 8: Vertical profiles of IWC and longwave radiative heating rate, Qir, for standard Cold (Cnir) and Warm (Wnir) simulations

the initial 10 minute diagnostic averaging period and then remaining almost constant through the remainder of the run.

All three of the models MetOffice, PSU and GSFC_L (Brown, Boehm and Lin) assume an initial diameter for newly nucleated ice crystals of about 1 micron. It appears that the slow initial rate of increase of IWP in the PSU and GSFC_L models is due in large measure to the reduced ice number concentration and hence the reduced crystal surface area available for the uptake of supersaturated water vapour. A further contributing factor to the slow IWP growth rate of PSU and GSFC_L is that the explicit microphysics scheme of these models takes account of surface kinetic effects which significantly reduce the growth rate of small crystals. These effects are not included in any of the typical bulk water microphysical schemes.

3.3 Time evolution of cloud boundaries

The time evolution of cloud top and base altitudes represent another gross feature of the simulations which can easily be compared. The models are all initialized with common temperature and water vapour profiles (the latter to within the accuracy of the different saturation vapour pressure relationships employed by them). Since the simulations are forced only by large-scale temperature changes, it is expected that the cloud top and base will respond principally to:

1 increases in the mean relative humidity profiles due to cooling with the water vapour profile conserved, and

2 redistribution of water vapour due to the presence of the cloud, caused by ice fallout below the cloud layer and upward mixing of water vapour by turbulence at the cloud top.

The first of these effects may be calculated simply by taking the initial temperature profile, cooling it in response to the large-scale forcing and then calculating its saturation mixing ratio. We may then calculate what will hereafter be referred to as "potential cloud top/base" altitudes as the upper and lower altitudes for which the initial mixing ratio profile exceeds the saturation value.

Figure 9 shows the cloud base and top altitudes for all standard warm and cold simulations at 4 hours, at the end of the period in which the models are forced. Also shown on the figure are the potential cloud top and base altitudes determined from the excess over ice saturation and, on the cloud top plot, the potential cloud top calculated w.r.t. water saturation. A number of points may be noted from Figure 9. Firstly, for the majority of the CRMs, the cloud top does not exceed the upper limit of ice saturation. Since some of these models allow ice nucleation whenever ice saturation is exceeded, this must imply that ice fallout plays a major role in removing ice mass from the cloud top region and hence reducing the cloud top altitude from its potential upper limit.

The MetOffice standard run allows nucleation only when water saturation is achieved. However, in this run the cloud top altitude exceeds that of the layer which will have been brought to water saturation by the forcing. This implies that there must have been some upward turbulent transport of water vapour. Examination of the water budget terms for this simulation confirms that this is the case.

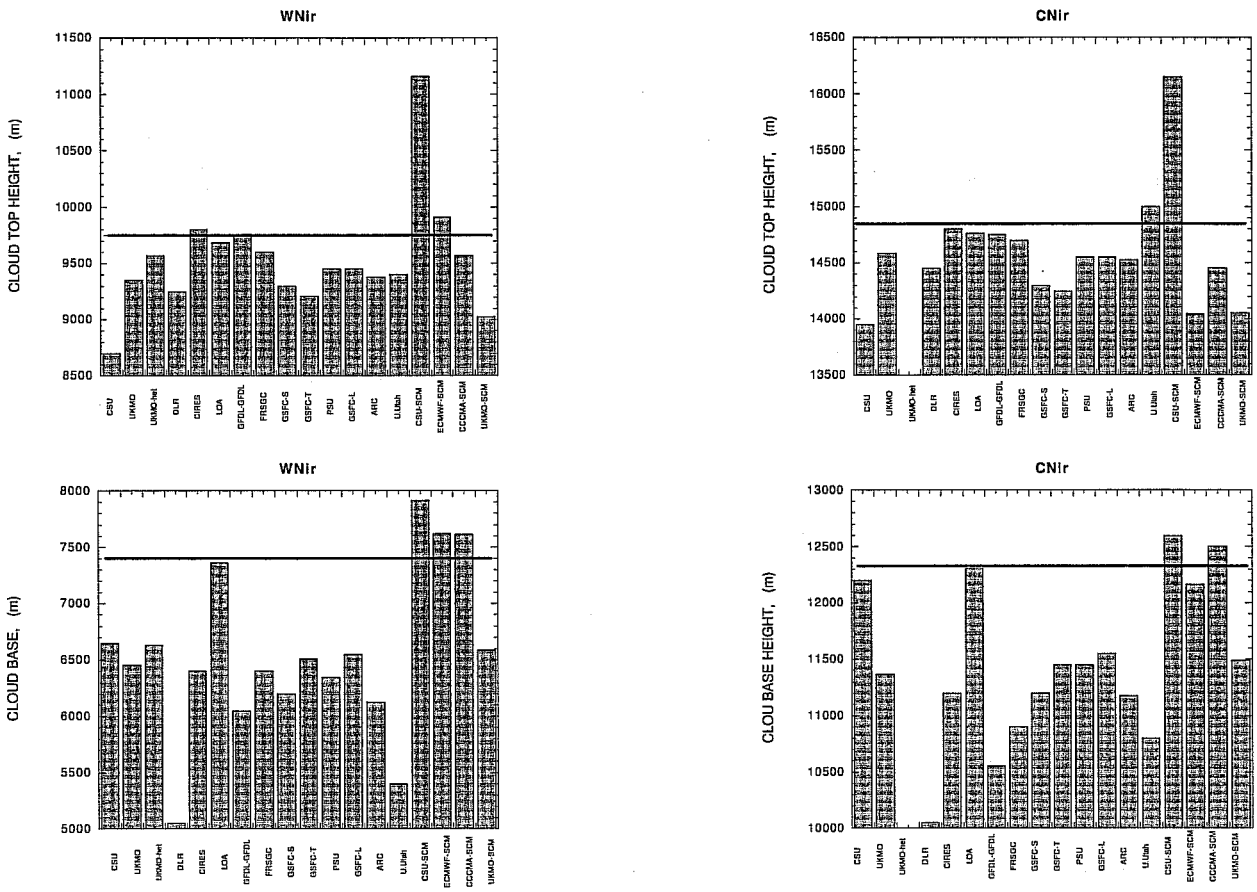

Figure 9: The distribution of cloud base (lower panels) and cloud top (upper panels) altitudes after four hours in the standard Cold (upper) and Warm (lower) simulations of the ICMC. The horizontal line in each case indicates the potential cloud top or base altitude, ie. the boundaries of the layer which exceeds ice saturation after cooling the initial moisture profile.

From the potential cloud top and base altitudes, we may calculate a potential IWC and vertically integrated IWP. Since this is derived simply from the excess mixing ratio over saturation it represents the IWC that would be obtained in the absence of any ice fallout or turbulent mixing. It also ignores any additional net cooling of the cloud layer due to radiative processes or net heating due to the release of latent heat, but does give some guidance as to the upper limit of IWC and IWP that will be expected in each case. At times of 0, 2 and 4 hours, the potential IWP has values of 20.2, 67.5 and 123.1 gm-2, respectively. The profile of potential IWC at 4 hours is shown in Figure 10. It is significant that this profile has a peak which is closer to the base of the layer, in common with the "bottom-peaked" IWC profiles shown in Figure 8, a function simply of the temperature dependence of the saturation mixing ratio. From this, it may be deduced that any model in which the peak IWC occurs at a higher altitude than that of the peak potential IWC must, therefore, have significant upwards transport of ice, such that the mean ice fallspeed in the updraught cores is less than the updraught strength itself.

Since we know that the majority of models have cloud bases which are below the potential cloud base, we expect that they will all have IWP below the potential IWP since cloud ice must have precipitated and evaporated into the unsaturated region below the potential cloud base. Evaporation of ice will cool the layer between potential and actual cloud bases, thus any attempt to calculate the reduction in IWP by evaporation in the initially subsaturated region below cloud must take account of this additional cooling. We assume that a layer in this initially subsaturated region has initial temperature and water vapour mixing ratio of T_0 and Q_0, respectively, where Q_0 is equal to the initial water vapour profile of the simulation and T_0 is the initial

temperature profile modified by large-scale ascent. After evaporation of ice, it has a final temperature, T_1, and is saturated at this temperature, hence

$$T_0 - T_1 = \frac{L_s}{C_P(Q_{sat,i}(T_1) - Q_0)} \tag{8}$$

This is solved iteratively for T_1. The amount of ice that is required to be evaporated in order to saturate the region between potential cloudbase (*Zpot*) and actual cloudbase (*Zbase*) may then be determined from

$$\Delta IWP = \int_{Zbase}^{Zpot} \rho_a (Q_{sat,i}(T_1) - Q_0) dz \tag{9}$$

The residual *IWP* remaining in the cloud layer is then simply the difference between potential *IWP* and *ΔIWP* . Values of potential *IWP* and *ΔIWP* for various actual cloudbase altitudes in the warm and cold cases are given at 4 hours in Table 3. Additionally, values of potential IWP at hourly intervals are plotted in Figure 7. For the warm case, the majority of models have actual cloud bases between 6.2 and 6.6 km suggesting that the range of IWP at 4 hr should lie somewhere between about 5 and 72 gm-2. This is in good general agreement with the results shown in Figure 7.

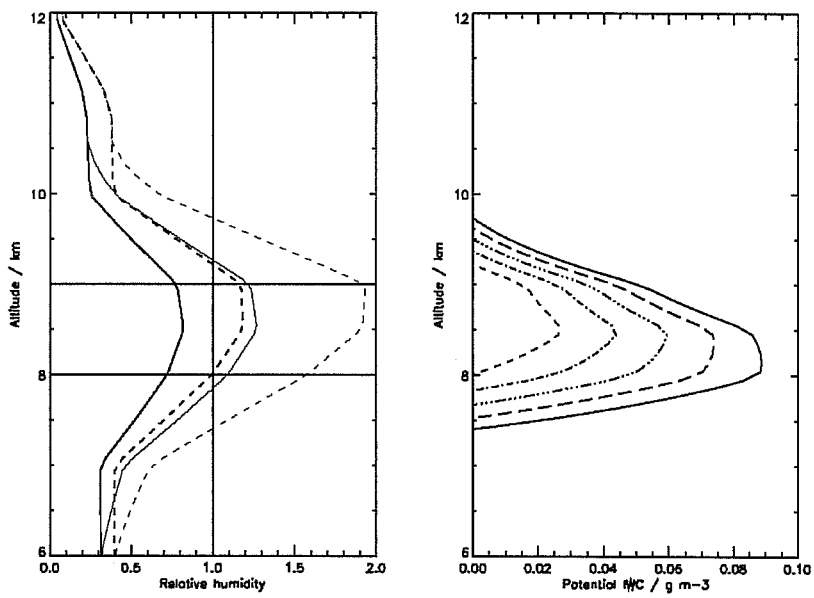

Figure 10: The left panel shows relative humidity w.r.t. ice (solid lines) and water (dashed lines). Darker lines are the initial values whilst the grey lines are the result of large-scale cooling of the domain for 4 hours. Right panel shows the potential IWC profile (ie. the excess water vapour mixing ratio above the saturation value) at times of 0,1,2,3 and 4 hours (left to right).

If the potential IWP values in Table 3 are compared with the time-series shown in Figure 7, it may immediately be seen that one of the models, LOA (Giraud), generates IWP values very close to the potential IWP. It is also notable that this model has cloud top and base altitudes which are close to the potential values. Its IWC profile is, however, one that is "top-peaked" (see Figure 8). Ice fallspeed diagnostics were not available from this model, but it easy to deduce that it has a tendency to produce low values. Little ice is lost from the cloud layer by precipitation and evaporation and the top-peaked profile is maintained by the upward turbulent transport of ice and vapour producing IWC profiles that are reminiscent of the LWC profiles found in stratocumulus cloud.

WARM CASE		
Potential cloud base [km]	Potential IWP [g m-2]	
7.41	123.1	
Actual cloud base [km]	ΔIWP due to evaporation [g m-2]	Residual IWP [g m-2]
7.0	9.1	114.8
6.8	26.2	97.7
6.6	51.0	72.9
6.4	79.6	44.3
6.2	118.7	5.2
6.0	164.0	
COLD CASE		
Potential cloud base [km]	Potential IWP [g m-2]	
12.34	17.3	
Actual cloud base [km]	ΔIWP due to evaporation [g m-2]	Residual IWP [g m-2]
12.0	1.8	15.5
11.7	6.7	10.6
11.4	14.5	2.8
11.1	26.1	
10.8	41.9	
10.5	61.4	

Table 3 For the Cold and Warm cases, the table shows the potential cloud base and ice water path (IWP), ie. the cloud base altitude and IWP that would be obtained by condensing any water vapour resulting from an excess over saturation with respect to ice in the temperature profile that exists after 4 hours of forced cooling. Additionally, the table shows the IWP deficit ie. the amount of ice water that must be evaporated to saturate the region between the potential cloud base and a lower cloud base altitude. The residual IWP is that part of the potential IWP that remains after evaporation of the IWP deficit.

We should not expect perfect correspondence between the models' cloudbase and residual IWP. IWP will be reduced by the impact of entrainment of sub-saturated air from above cloud-top. Additionally, some of the models will be able to maintain a layer near cloudbase in which ice exists in unsaturated air. This is likely to be the case in those models that distinguish between small pristine ice crystals and larger particles such as aggregates. The latter, having higher fall velocities, will penetrate further in unsaturated air before evaporating completely. From such a model, we would diagnose a lower cloudbase and a higher IWP than that given by the simple analysis above. Significant penetration of precipitating ice into unsaturated air is indicated by those IWC profiles which do not have a sharp cutoff at cloudbase but decline more slowly to zero. For cold case simulations, a number of models have a cloudbase below 11.4 km but IWP above the lowest residual value in Table 3. This suggests that these models have significant penetration of falling ice into unsaturated air.

A group of such models includes MetOffice, DLR and GFDL (Brown, Gierens, and Koehler), all of which are capable of representing large ice in either bulk form or in explicit size bins. DLR represents a rather extreme case in which an initial population of ice particles falls rapidly out of the initial cloud layer and then

evaporates very slowly. It has a cloud base below 5 km after 4hr but IWP of around 35 gm-2. IWC profiles from GFDL all exhibit a characteristic kinked behaviour in the cloudbase region. This represents the altitude at which all small ice has been completely evaporated, leaving only larger ice to persist in subsaturated air below this level.

Another possible cause of non-correspondence between actual IWP and the residual IWP predicted above for a given cloudbase altitude is the existence of sub- and supersaturation within the cloud layer. These can exist in downdraught and updraught regions, respectively, within the neutrally-stable layer. Supersaturation will also exist in the stable layer below this that has been moistened by the evaporation of precipitating ice. This layer continues to be cooled by the large-scale forcing and is, therefore, a region of ice particle growth. In the MetOffice model, both sub- and supersaturated points occur in the turbulent layer between 8 and 9 km with a slightly supersaturated region below 8km. Supersaturation also exists above 9 km since this model only allows nucleation to occur once water saturation has been achieved.

3.4 Impact of LW radiation and static stability

It is expected that differential radiative heating across the cloud layer will be one of the significant sources of turbulent kinetic energy in the simulated clouds. The ability of this heating to generate turbulence will be constrained by the static stability of the initial temperature profile, so we may consider these factors together to some extent.

Figure 8 also shows the vertical profiles of long-wave radiative heating for each CRM for both warm and cold cases. It is clear that there is a wide variety of behaviour amongst the participating models. Again, we will not seek to describe all these differences completely but attempt to isolate some general aspects of the model behaviour.

In the Warm case, the models PSU, MetOffice, GSFC_L and GSFC_T (Boehm, Brown, Lin, Wang/Tao) generate IWC profiles which peak towards the bottom of the cloud layer. The first three of these also have heating profiles in which warming due to the absorption of radiation from the surface and or underlying atmosphere is concentrated in the region around the IWC peak altitude, with a deeper layer of cooling above. These contrast with the models DLR, LOA and FRSGC (Gierens, Giraud and Maruyama), in which there is a well-defined IWC peak near to the cloud layer top. In this case, the LW cooling is also concentrated close to the cloud top, and the LW heating profile provides cooling at the top and warming at the base of the 8-9km neutrally-stable layer.

All of these models do, however, exhibit lower levels of vertical velocity variance in the no-radiation case so it is clear that the existence of a cooling-heating dipole across the neutrally-stable layer is not a simple criterion for the model being dynamically active. Pre-existing structure in the cloud ice field will lead to horizontal gradients in the latent heating due to microphysical processes that will also act to maintain turbulent motions in the neutrally-stable layer.

All the participating CRMs use their own radiation schemes and methods of deriving cloud radiative properties from their microphysical fields. There is, therefore, scope for differing feedbacks between microphysical and radiative processes which complicates the interpretation of all the model results. However, some insight may be gained by examining the impact of changing IWC profiles on the radiative heating profiles generated by one of the models. Figure 11 shows some simplified IWC profiles, chosen to represent most of the features seen in the profiles at Figure 8 Temperature and moisture profiles are taken form the MetOffice CRM simulation at 4 hours (ie. the end of the forcing. Also shown are the LW radiative

heating profiles calculated assuming the ice is comprised of spherical particles of effective radius 30 μm. This confirms that, to first order, the shape of the LW heating profile is related simply to the IWC profile. Thus, a bottom-peaked IWC profile has warming concentrated near cloudbase, whilst a top-peaked profile has cooling concentrated near cloudtop.

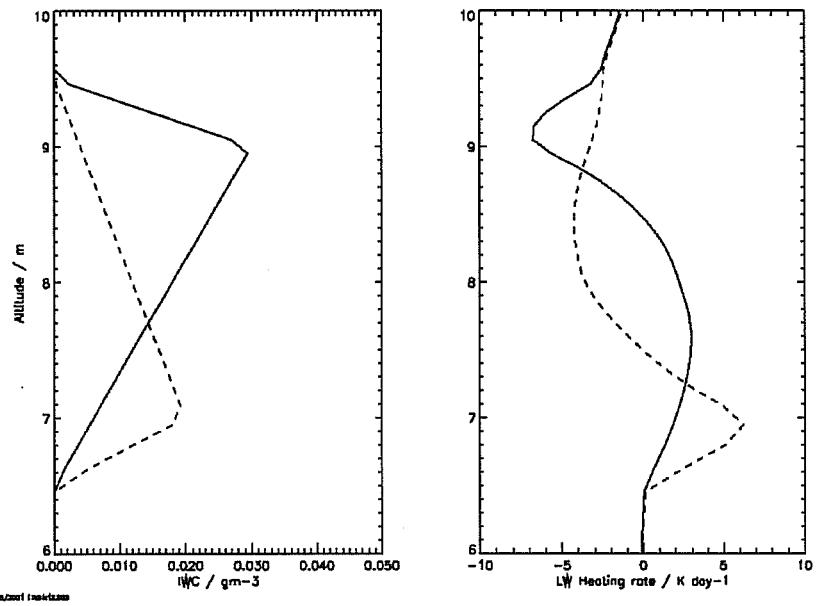

Figure 11: The right panel shows longwave radiative heating rates calculated by the radiation scheme from the Met Office CRM using the ICMC initail profiles of temperature and water vapour mixing ratio. Solid and dashed lines are derived from the two sample IWC profiles shown in the left panel, assuming that the ice consists of spherical particles with an effective radius of 30 μm.

The model GSFC_T (Wang/Tao) then appears to be of interest in that it has a bottom-peaked IWC profile but with a shallow layer of LW cooling which is acts to generate instability over the 8-9km layer. Based on the above simplified radiative heating calculations, this may be understood if the particle effective radius near the cloud top is reduced below 30 μm, so as to increase the optical depth of the upper part of the cloud layer. Of the models with a prognostic ice number concentration, this model generates the largest values, thereby giving the required smaller mean particle sizes for a given IWC.

In nearly all the simulations run with an initial statically stable temperature profile, turbulence was suppressed throughout the simulation. For models that were turbulent in the standard case, this in turn reduced the degree of structure in the horizontal distribution of IWP. The main exception to this was the LOA model (Giraud). In this case, its ability to retain most of the potential IWP gave cloud-top LW cooling rates which were sufficient to destablize the cloud layer between 2 and 3 hr into the simulation.

3.5 Impact of fixed ice fallspeeds

For models with a prognostic number concentration for ice hydrometeors (either bulk or explicit schemes), the production of higher values will give smaller mean particle sizes, and hence smaller mean ice fallspeeds, for a given IWC. The use of a fixed fallspeed for ice effectively removes any feedbacks between the simulated ice nucleation processes and their sensitivity to cloud dynamics on the ice fallspeed. It also

removes any potential differences between models due to their choice of different parameter values to describe the mass and fallspeed of a single ice crystal.

Model	Fallspeed = 20 cm s^{-1}		Fallspeed = 60 cm s^{-1}	
	Cold	Warm	Cold	Warm
PSU (Boehm)	1.2	2.5	0.6	1.0
MetOffice (Brown)	2.0	2.8	0.7	0.8
DLR (Gierens)	2.7	3.0	0.6	1.2
LOA (Giraud)	0.7	0.8	0.3	0.3
GFDL (Koehler)	1.7	1.5	1.0	1.0
GSFC_L (Lin)	1.2	2.3	0.5	1.0
GSFC_S (Starr)			4.7	1.0
GSFC_T (Wang/Tao)	2.0	4.8	1.4	2.3

Table 4 The ratio of IWP in fixed-fallspeed runs to IWP in standard model, after 4 hours.

The gross impact of running a number of the models with fixed ice fallspeeds is illustrated in Table 4, which gives the ratio of IWP in the fixed-fallspeed run to that in the standard run, for the two values of fallspeed that were used (20 and 60 cm s^{-1}). The value of 20 cm s^{-1} always acts to increase the IWP, except for the LOA model (Giraud) which in the standard run has almost no ice precipitation from the cloud layer, and hence a very low effective ice fallspeed.

Figure 12 shows the evolution of the vertical profiles of IWC in both Cold and Warm cases for the models LOA and MetOffice (Giraud and Brown). For the MetOffice model, the effect of using a fixed 20 cm s^{-1} fallspeed is to alter the shape of the IWC profile from bottom- to top-peaked. This in turn allows a radiative heating gradient to be maintained across the neutrally-stable layer in both warm and cold cases, resulting in greatly-increased values of the mean vertical velocity standard deviation, which exceed the fixed ice fallspeed, hence the conversion to a top-peaked IWC profile. Both models also show a characteristic minimum in IWC around 8km altitude in the Warm case and 13km in the Cold case. This is the base of the neutrally-stable layer and is therefore the lowest level in the cloud which is affected by radiatively driven turbulent motions, ice being evaporated in the downdrafts. The LOA model (Giraud) is converted from a top-peaked IWC profile in the control run to a bottom-peaked profile with ice fallspeed of 60 cm s^{-1}. This value exceeds the mean W_{RMS} and so ice accumulates at the base of the cloud layer, giving a similar structure to the MetOffice model (Brown) in which generates mean fallspeeds closer to 60 cm s^{-1} throughout the run.

3.6 Mesoscale dynamical impact of ice-phase microphysics

Recent work in WG3 has concentrated on simulations of an observed case from the Fronts and Atlantic Storm Tracks Experiment (FASTEX, Joly et al. 1997). The case is that of a developing frontal wave, from (date), referred to as FASTEX IOP16 of 17/2/97 Clough et al. (2000) have identified the role of diabatic cooling produced by the evaporation of precipitating ice in reinforcing cross-frontal circulations in this case, and hence affecting the intensity of the developing system. Simulations of this case may, therefore, be expected to show sensitivity to the way in which the ice phase microphysics scheme of the model is able to reproduce both the correct magnitude and vertical scale of the evaporative cooling.

In order to examine this process, participating models (which are essentially versions of operational mesoscale NWP models) were run with sensitivity tests to doubling/halving both the ice fallspeed and depositional growth rate. Diffusional growth or evaporation of precipitating hydrometeors is enhanced by the

so-called "ventilation coefficient", the factor by which the diffusion of heat and water vapour to or from the particle is increased above that for a non-precipitating particle. An arbitrary increase of the depositional growth rate is, therefore, representative of the impact of distributing the model's ice hydrometeors into a spectrum of larger, faster-falling particles, whilst maintaining the original mass-weighted fallspeed for the purposes of calculating the precipitation rate.

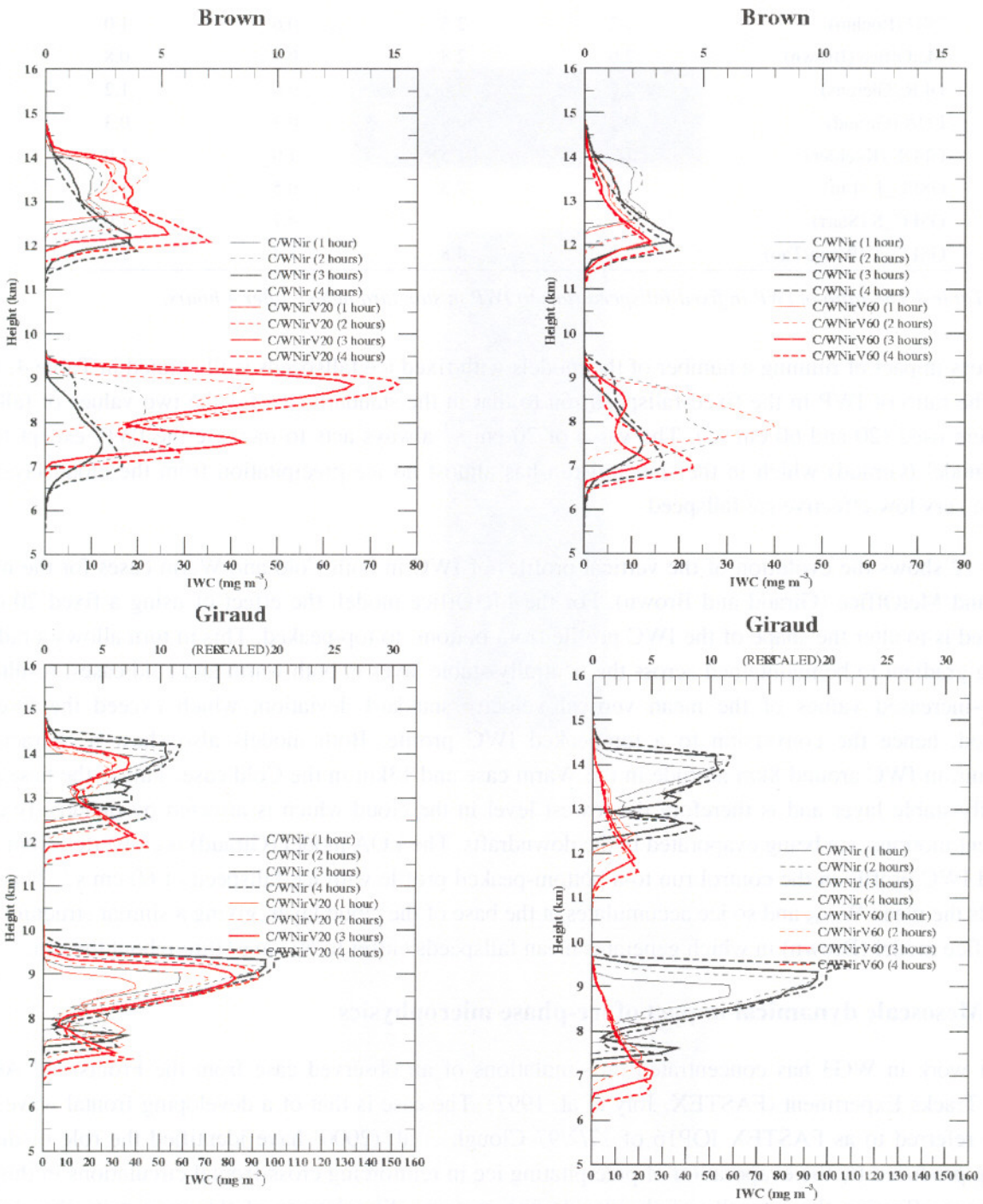

Figure 12: Each panel shows IWC profiles at 1,2,3 and 4 hours from standard and fixed ice fallspeed simulations. Results from Warm cases are plotted below 10km on the vertical axis with Cold cases above. Upper panels show results from the Met Office model (Brown) whilst the lower panels show results from the LOA model (Giraud). V20 and V60 indicate the fixed fallspeeds of 0.2 and 0.6 ms^{-1}, respectively.

The impact of these factors will be illustrated in simulations using the Met Office Unified Model (UM). The simulations were run with a version derived from the operational mesoscale version of this model. It had 310*210 gridpoints in the horizontal with 0.105 degree resolution (approximately 12km) and 45 levels in the vertical compared to the 38 of the operational version. This gave layer thicknesses of around 30 hPa in the mid-troposphere compared to 50 hPa in the operational version. The model was initialised using the analysis from the operational Limited Area Model at 18Z on 16/2/97 so that there was little initial mesoscale structure. The large-scale precipitation scheme of the model is described by Wilson and Ballard (199x) and has a single prognostic variable to describe all ice phase hydrometeors. This is assumed to be distributed in an exponential size spectrum with the total number concentration being described by a function increasing with decreasing temperature, hence representing the broadening of the spectrum at lower levels due to processes such as aggregation.

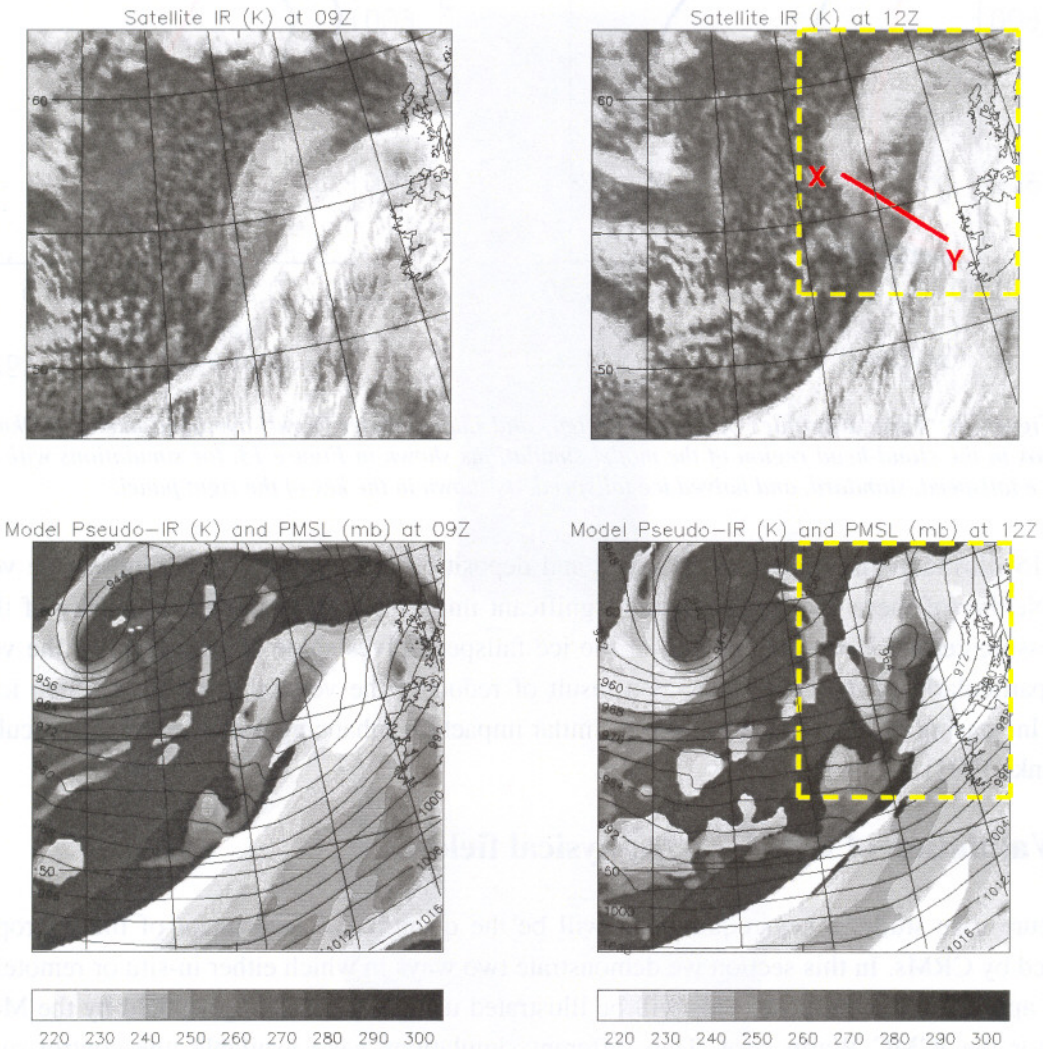

Figure 13: Upper panels show Meteosat IR cloudtop temperature at 09 and 12Z for the FASTEX IOP16 case. Below are simulated cloudtop temperatures from the Met Office mesoscale model simulation for the same times.

Figure 13 shows a comparison of observed infra-red cloud-top temperatures with those simulated from the model. This confirms that the simulation generates one of the main characteristic features of the system, a developing cloud-head (Pascoe 1993). Figure 14 shows vertical profiles of ice and liquid hydrometeors averaged over a 300km square region within the cloud-head. Doubling (halving) of the ice fallspeed results in an approximate halving (doubling) of the mean IWC. Additionally, the reduced ice storage above the

freezing level resulting from doubled ice fallspeed results in a reduced uptake of water vapour by the ice phase and hence increases the water content of supercooled liquid cloud.

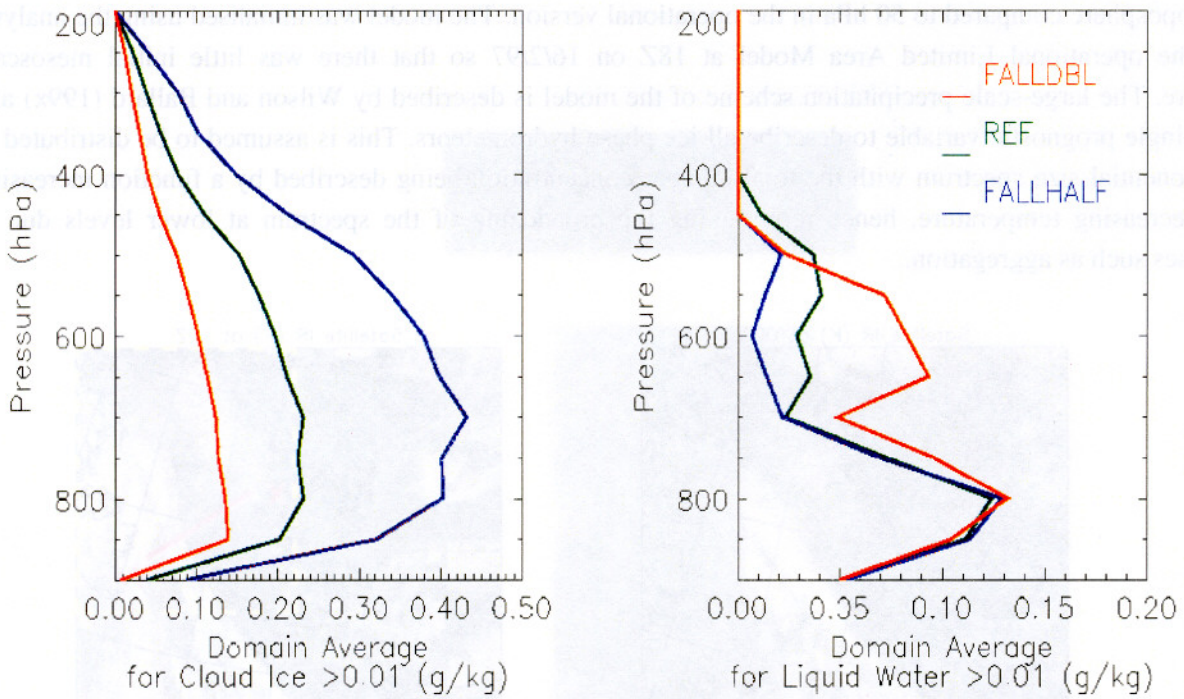

Figure 14: Vertical profiles of Cloud Ice (left) and Liquid Water (right) averaged over a 300km square box in the cloud-head region of the model simulations shown in Figure 13, for simulations with doubled ice fallspeed, standard, and halved ice fallspeed, as shown in the key of the right panel.

Figure 15 illustrates the impact of fallspeed and deposition rate changes on the mesoscale vertical motion fields. Neither of these changes have any significant impact on the position or intensity of the developing low pressure centre. However, halving of the ice fallspeed gives some enhancement of the vertical motion fields, particularly in the cold front, as a result of reducing the vertical scale over which ice evaporation occurs. Increasing the deposition rate has a similar impact on enhancing the direct frontal circulation (Clough and Franks 1991).

4. Validation of CRM microphysical fields

In a future case study, a key requirement will be the quantitative assessment of the microphysical fields generated by CRMs. In this section we demonstrate two ways in which either in-situ or remotely-sensed data may be applied to this purpose. This will be illustrated using CRM fields generated by the Met Office LES model for the ICMC Warm case. Two different simulations were available, the control run (referred to hereafter as HOM), in which nucleation by homogeneous freezing of liquid droplets was allowed at water saturation and for T < -38C, and a run in which heterogenous ice nucleation following the scheme of Meyers et al. (1992) was represented (referred to hereafter as HET). The HET run forms ice from the start of the simulation, whereas in the HOM run, ice only appears after 90. This delay represents the time required for the imposed large-scale cooling to bring the neutrally-stable layer to water saturation, allowing the subsequent diagnosis of supercooled liquid water and its transfer to the cloud ice species due to homogeneous freezing. Between 90 and 130 minutes, approximately 50% of the total ice water path in the

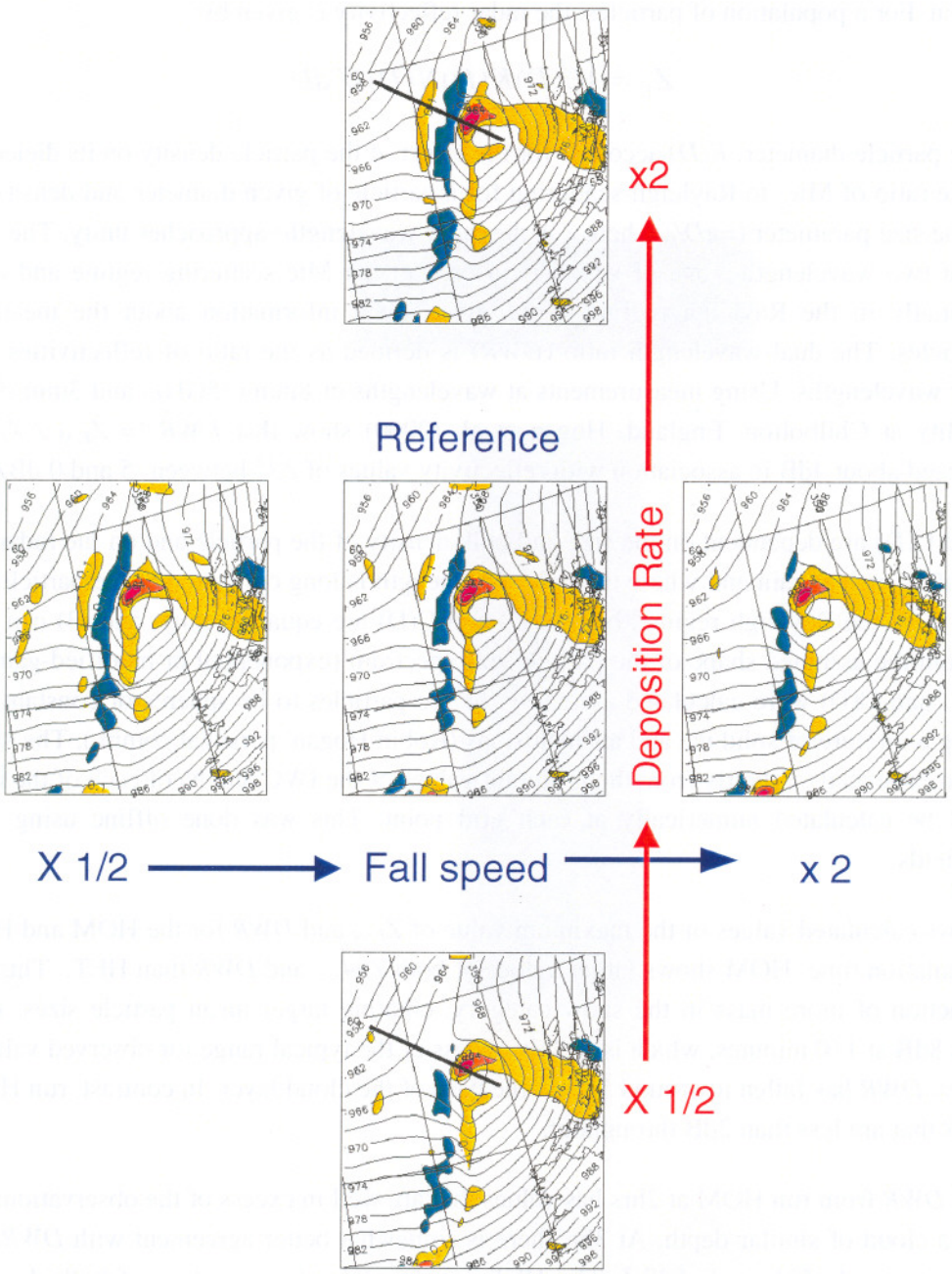

Figure 15: Vertical velocity (m/s) at 800 hPa at 12Z in Met Office mesoscale model simulations of FASTEX IOP16. The centre panel shows the control simulation, with those having doubled and halved ice fallspeeds and deposition rates as indicated.

HOM run is in the snow species, whereas in the HET run, all the ice remains in the cloud ice (pristine crystals) category.

Hogan et al. (2000) describe the use of dual-wavelength radar measurements for the retrieval of ice particle size information. For a population of particles, the radar reflectivity is given by:

$$Z_E = \int C(D)K(D)N(D)D^6 dD \tag{10}$$

where D is the particle diameter, $K(D)$ accounts for the effect of the particle density on its dielectric constant and $C(D)$ is the ratio of Mie- to Rayleigh-scattering for a particle of given diameter and density. This factor decreases as the size parameter ($=\pi D/\lambda$ where λ is the radar wavelength) approaches unity. The ratio of radar reflectivities at two wavelengths, one of which is in or near the Mie scattering regime and one of which remains essentially in the Rayleigh regime hence gives some information about the mean size of the scattering particles. The dual-wavelength ratio (DWR) is defined as the ratio of reflectivities made at two different radar wavelengths. Using measurements at wavelengths of 8mm (35GHz) and 3mm (94GHz) from the radar facility at Chilbolton, England, Hogan et al. (2000) show that DWR ($= Z_{E,35} / Z_{E,94}$) does not commonly exceed about 4dB in association with reflectivity values of $Z35$ between -5 and 0 dBZ.

Both K(D) and C(D) are dependent on the size and bulk density of the particle and on the radar wavelength. For water droplets such as rain and where the radar wavelength is long compared to the particle diameter, so that scattering is in the Rayleigh regime, both K(D) and C(D) are equal to unity, and (3) can be evaluated analytically from the assumed shape of the particle size spectrum (exponential or modified-gamma). For ice particles, K(D) and C(D) were calculated assuming the ice particles to be spheres of constant bulk density and comprising a mixture of solid ice and air inclusions (Robin Hogan, personal comm.). The size spectrum, N(D), was then evaluated explicitly from the gridpoint values of the IWC and N_I of each of the ice species so that (3) could be calculated numerically at each grid point. This was done offline using saved model hydrometeor fields.

Figure 16 shows calculated values of the maximum value of $Z_{E,94}$ and DWR for the HOM and HET runs at 2 and 3hr of simulation time. HOM shows larger values of both $Z94_{max}$ and DWR than HET. This is consistent with its production of more mass in the snow category, creating larger mean particle sizes. DWR for run HOM exceeds 8dB at 110 minutes, which is well in excess of the typical range for observed values of 0-4dB. At 180 minutes, DWR has fallen to around 5dB at the base of the cloud layer. In contrast, run HET generates values of DWR that are less than 2dB throughout.

The simulated DWR from run HOM at 2hrs has values that are well in excess of the observations of Hogan et al. (2000) for a cloud of similar depth. At 3hr, there is somewhat better agreement with DWR_{max} of around 4dB in association with $Z94_{max}$ of -6dBZ. The HET run maintains lower values of both these parameters throughout and does not approach the values of DWR_{max} seen in observations.

At each model grid point, the parametrized size spectra of cloud ice and snow may be evaluated using the prognosed values of mass and number concentration for each species. The total ice mass due to all particles smaller and larger than 500 mm in diameter may then be determined. Model results from the HOM and HET simulations are shown in Figure 17. Also shown in this figure are observational data obtained during Lagrangian spiral descents, in which the sampling aircraft descends at an average speed of around 1 ms^{-1} whilst drifting with the mean horizontal wind so as to track the evolution of a population of falling particles. These observations were obtained in mid-latitude frontal cirrus cloud bands and are described more fully by Field (2000).

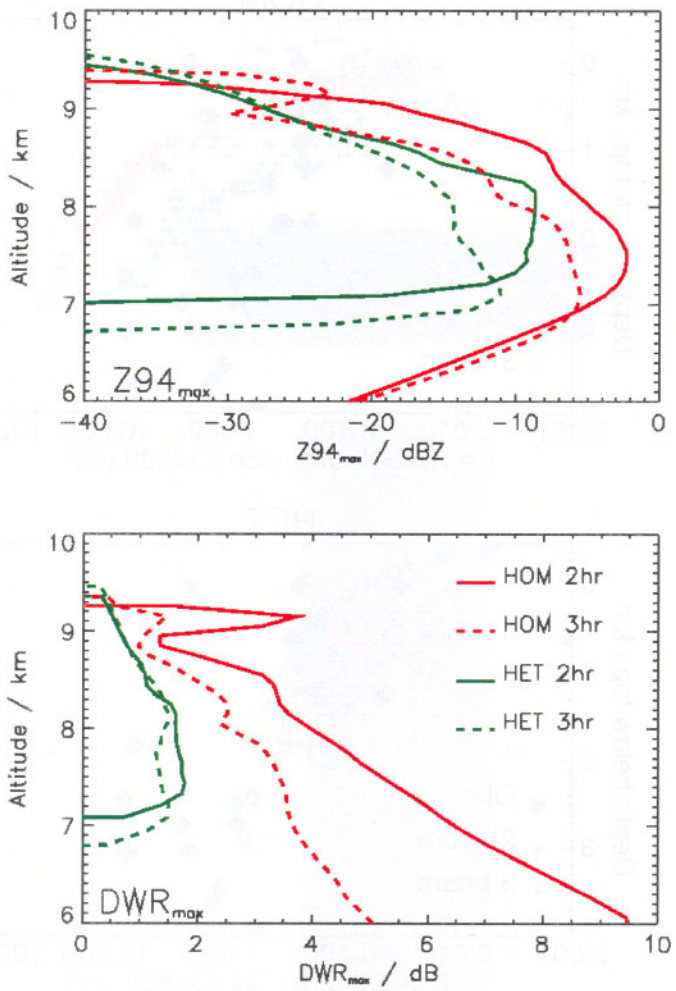

Figure 16: Simulated 94 GHz radar reflectivity, Z94, and dual-wavelength ratio, DWR, from simulations of the ICMC Warm case by the Met Office CRM. Vertical profiles of the maximum values occurring within the model domain at times of 2 and 3 hr are shown, HOM indicates a simulation in which homogeneous freezing of liquid water was simulated at temperatures colder than -38C. HET indicates a run which used the Meyers et al. (1992) parameterization of heterogenous IN activation.

Although the observations of large- to small-particle ice mass contribution have a large scatter, they suggest that the model results from HOM at 3hrs have a somewhat better agreement than at 2hrs. In particular, the rate of increase of large particle mass with depth below cloud top appears to be too rapid. In contrast, large particle mass in the HET run appears to be too low throughout the run.

Taken together, these results suggest that the peak of snow formed immediately following cloud formation in HOM is probably spurious. In this run, nucleation can only occur in regions that have achieved saturation w.r.t. water. The use of random initial temperature perturbations on the grid scale ensures that saturation brought about by the uniform cooling of the domain tends to occur initially in regions which have a horizontal scale comparable with that of the grid. This leads to sharp gradients in the ice number concentration. It appears that numerical diffusion of these concentration gradients can lead to the attribution of mass-mean cloud ice diameters that exceed the 500 μm threshold for the onset of autoconversion to snow,

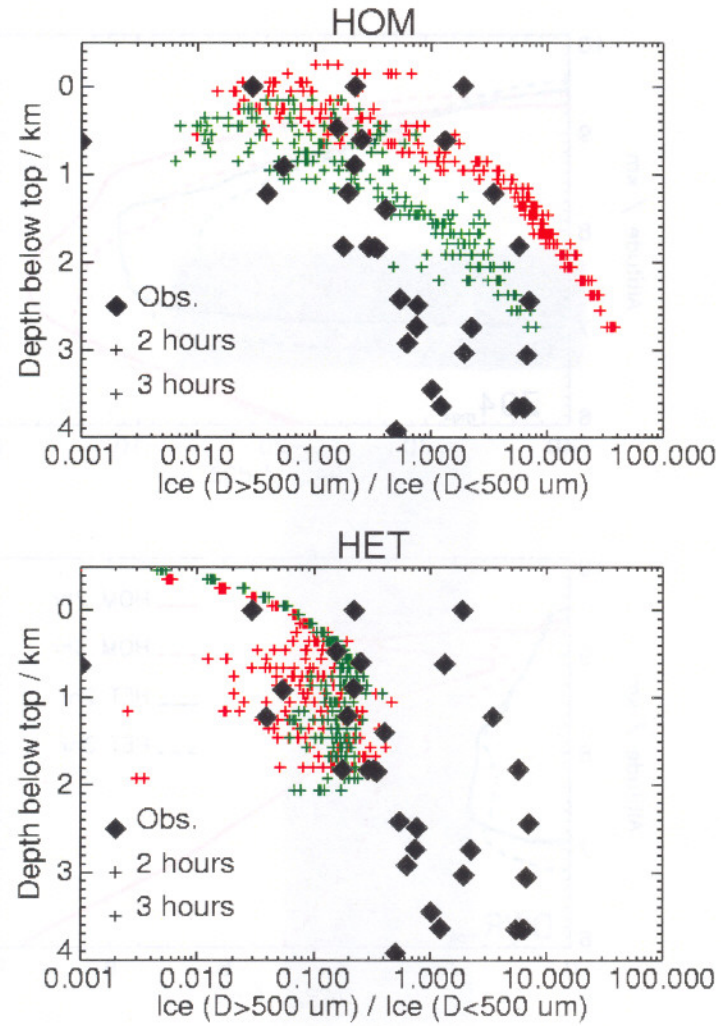

Figure 17 The x-axis shows the ratio of IWC in particles larger than 500 μm diameter to that in particles smaller than 500 μm. Large solid symbols are aircraft observations from Lagrangian spirals in frontal cirrus (Field 2000), whilst crosses are from Met Office CRM runs of ICMC Warm case at 2 and 3 hr. HOM and HET model runs are as described in Figure 16

which can then grow further by deposition and accretion of cloud ice. In the HET run, the initial ice concentrations (approx. 10^5 kg^{-1}) are much less than those of the HOM run (approx.10^8 kg^{-1}). They are, however, much more uniform over the domain and this problem does not occur. It is planned to provide the model with a new parametrization of homogeneous freezing based on results from the Met Office 1-d parcel model (Spice et al. 1999, Cotton and Field 2000), with a view to improving this aspect of model behaviour.

Another feature of the HOM run which contrasts with that seen in observations is the relatively slow decrease in maximum radar reflectivity towards the cloud base. This suggests that the ice mass contained in larger, more rapidly-falling snow particles is not evaporating sufficiently rapidly when it falls into sub-saturated air. The behaviour of the HET run appears to be better in this respect.

In the FASTEX IOP15 case, described in section 3.6 above, single wavelength radar reflectivity measurements were available from the conically-scanning ELDORA system carried on the NCAR Electra aircraft. A comparison of observed radar reflectivity with that simulated from the model hydrometeor fields (Figure 18) suggests that the simulation with doubled ice fallspeed is giving the most realistic range of values.

This study illustrates how the availability of both in-situ particle size measurements and, ideally, dual-wavelength radar measurements in a future case study can be used to guide the improvement of the model's microphysics scheme. Since the information about mean particle sizes that is provided by *DWR* measurements can also be obtained from in-situ data, the availability of dual-wavelength radar is not crucial. It does, however, provide a more representative view of the evolving vertical structure of the cloud than can be obtained from aircraft measurements at a single level.

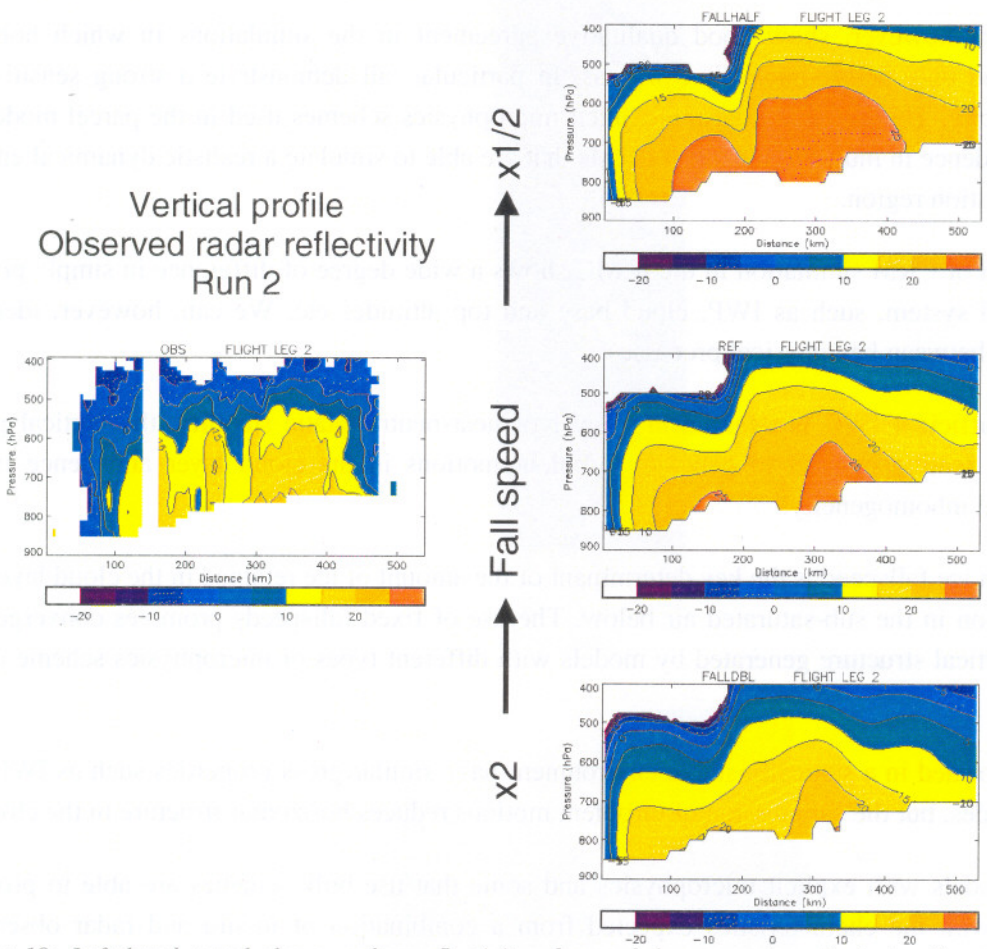

Figure 18: Left hand panel shows radar reflectivity observed from an aircraft during Run 2 of the FASTEX IOP16 case. The right hand panels show radar reflectivity simulated from hydrometeor fields simulated by the Met Office mesoscale model for the runs with halved (upper), standard (middle) and doubled (lower) ice fallspeeds.

5. Summary and Conclusions

The CPMC study has identified the major causes of disagreement between 1-d parcel nucleation models. These are:

i) the representation of the homogeneous freezing rate of haze droplets,

ii) the treatment of the solute concentration in haze droplets,

iii) the growth rate of the crystals once nucleated, and in particular the effect of the accommodation coefficient, β_I on the growth rate of small crystals.

iv) The availability and mode of activity of heterogeneous IN.

The models did, however, show good qualitative agreement in the simulations in which homogeneous freezing was the only active nucleation process. In particular, all demonstrate a strong sensitivity to the updraught velocity. This suggests that the explicit microphysics schemes used in the parcel models may be used with confidence in multi-dimensional CRMs that are able to simulate a realistic dynamical environment in a cirrus formation region.

The comparison of CRM simulation in the ICMC shows a wide degree of difference in simple properties of the cirrus cloud system, such as IWP, cloud base and top altitudes etc. We can, however, identify some important links between key physical processes:

i) Where sufficient IWC is retained in a layer of near-neutral static stability, the vertical gradient of radiative heating can act to generate turbulent motions in the cloud layer and hence increase its horizontal inhomogeneity.

ii) The mean ice fallspeed is the key determinant of the amount of ice retained in the cloud layer or lost to evaporation in the sub-saturated air below. The use of fixed fallspeeds promotes convergence in the mean vertical structure generated by models with different types of microphysics scheme (explicit or bulk).

iii) Clouds formed in a statically-stable environment have similar gross properties such as IWP, base and top altitudes, but the suppression of turbulent motions reduces horizontal structure in the cloud.

iv) Some models with explicit microphysics and some that use bulk schemes are able to produce IWC profiles with the characteristics expected from a combination of in-situ and radar observations of cirrus layers.

v) Models that have some means to distinguish between large and small ice particles (by means of either size bins or large-particle categories in bulk schemes) have greater depth scales for the evaporation of ice in subsaturated air.

Sensitivity tests with one model have demonstrated the potential impact of cloud microphysics on the mesoscale dynamics of mid-latitude frontal systems. In particular, the ice fallspeed and deposition rate both affect the vertical scale over which ice evaporation occurs below the cold front, with a consequent impact on the cross-frontal circulation. We may expect that CRM simulation, well-validated against observations will

provide good guidance on whether the bulk microphysics schemes implemented in larger-scale models have the appropriate sensitivity to the applied forcing to ensure realistic feedbacks between microphysics and dynamics in all parts of a weather system.

Acknowledgements

We would like to acknowledge the efforts of all those who have contributed results to the WG2 and WG3 studies:

Richard Cotton, Eric Jensen, Ken Sassen, Bernd Kaercher, Paul DeMott, Angela Benedetti, Matt Boehm, Klaus Gierens, Eric Girard, Vincent Giraud, Vitaly Khvorostyanov, Martin Koehler, Ken-Ichi Maruyama, Yansen Wang, Wei-Kuo Tao, Martin Montero, Ulrike Lohmann, Christian Jakob, Damian Wilson, Richard Forbes, Humphrey Lean, Klara Finkele, Jack Katzfey, Burkhardt Rockel, Peter Yau.

6. References

Clough,S.A. and R.A.A.Franks (1991) The evaporation of frontal and other stratiform precipitation. Q.J.R.Meterol.Soc., 117, pp1057-1080.

Clough,S.A., H.W.Lean, N.M.Roberts and R.M.Forbes (2000) Dynamical effects of ice sublimation in a frontal wave. Q.J.R.Meterol.Soc., 126, pp2405-2434.

DeMott,P.J. (2001) Laboratory studies of cirrus cloud processes, in Cirrus, edited by D.K.Lynch, K.Sassen and D.O'C.Starr, Oxford University Press, London (in press).

DeMott,P.J. and D.C.Rogers (1990) Freezing nucleation rates of dilute solution droplets measured between -30 deg and -40 deg C in laboratory simulations of natural clouds. J.Atmos.Sci., 47, pp1056-1064.

DeMott,P.J., M.P.Meyers and W.R.Cotton (1994) Parameterization and impact of ice initiation processes relevant to numerical model simulations of cirrus clouds. J.Atmos.Sci., 51, pp77-90

DeMott,P.J., D.C.Rogers and S.M.Kreidenweiss (1997) The susceptibility of ice formation in upper tropospheric clouds to insoluble aerosol components. J.Geophys.Res., **102**, pp19575-19584.

DeMott,P.J., D.C.Rogers, S.M.Kreidenweiss, Y.Chen, C.H.Twohy, D.Baumgardner, A.J. Heymsfield and K.R.Chan (1998) The role of heterogeneous freezing nucleation in upper tropospheric clouds: Inferences from SUCCESS. Geophys.Res.Lettt., **25**, pp1387-1390.

Field, P.R. (2000) Bimodal ice spectra in frontal clouds. Q.J.R.Meterol.Soc., **126**, pp379-392.

Fletcher, N.H. (1962) The physics of rainclouds. Cambridge University Press, London.

Fowler, L.D., D.A.Randall and S.M.Rutledge (1996) Liquid and ice cloud microphysics in the CSU General Circulation Model. Part I. Model description and simulated microphysical processes. J.Clim., **9**, pp489-529.

Gregory,D. and D.Morris (1995) The sensitivity of climate simulations to the specification of mixed phase clouds. Clim.Dynam., **12**, pp641-651.

Heymsfield, A.J. and L.M.Miloshevich (1993) Homogeneous ice nucleation and supercooled liquid water in orographic wave clouds. J.Atmos.Sci., **50**, pp2335-2353.

Heymsfield, A.J. and R.M.Sabin (1989) Cirrus crystal nucleation by homogeneous freezing of solution droplets. J.Atmos.Sci., **46**, pp2252-2264.

Hogan,R.M., A.J.Illingworth and H.Sauvageot (2000) Measuring crystal size in cirrus using 35- and 94-GHz radars. J.Atmos.Oceanic Technol., **17**, pp27-37.

Jeffery,C.A. and P.H.Austin (1997) Homogeneous nucleation of supercooled water: Results from a new equation of state. J.Geophys.Res., **102**, pp25269-25279.

Jensen, E.J. and O.B.Toon (1994) Ice nucleation in the upper troposphere: Sensitivity to aerosol number density, temperature and cooling rate. Geophys.Res.Lett., **21**, pp2-19-2022.

Jensen,E.J., O.B.Toon, A.Tabazedeh, G.W.Sachse, B.E.Anderson, K.R.Chan, C.W.Twohy, B.Gandrud, S.M.Aulenbach, A.J.Heymsfield, J.Hallett and B.Gary (1998) Ice nucleation processes in upper tropospheric wave-clouds observed during SUCCESS. Geophys.Res.Lett., **25**, pp1363-1366.

Joly,A., D.Jorgensen, M.A.Shapiro, A.J.Thorpe, P.Bessemoulin, K.A.Browning, J-P.Cammas, J-P.Chalon, S.A.Clough, K.A.Emanuel, L.Eymard, R.Gall, P.H.Hildebrand, R.H.Langland, Y.Lemaitre, P.Lynch, J.Moore, P.O.G.Persson, C.Snyder and R.M.Wakimoto. (1997) The Fronts and Atlantic Storm-Track Experiment (FASTEX): Scientific objectives and experiment design. Bull.Am.Meteorol.Soc., **78**, pp1917-1940.

Khvorostyanov, V. and K.Sassen (1998) Cirrus cloud simulation using explicit microphysics and radiation. Part I. Model description. Part II. Microphysics, vapor and ice mass budgets, and optical and radiative properties. J.Atmos.Sci., **55**, pp1808-1845

Krueger,S.M., Q.Fu, K.N.Liou and H-N.S.Chin (1995) Improvements of an ice-phase microphysics parameterization for use in numerical simulations of tropical convection., J.Appl.Meteorol., **34**, pp281-287.

Lin,H., K.J.Noone, J.Strom and A.J.Heymsfield (1998) Small ice crystals in cirrus clouds: a model study and comparison with in situ observations. J.Atmos.Sci., **55**, pp928-1939.

Meyers,M.P., P.J.DeMott and W.R.Cotton (1992) New primary ice nucleation parametrizatons in an explicit cloud model. J.Appl.Met., **31**, pp708-721.

Pascoe, M. (1993) Cloud heads - precursors to rapid cyclogenesis. Weather and Climate, **13**, pp10-16

Pruppacher,H.R. (1995) A new look at homogeneous ice nucleation in supercooled water drops. J.Atmos.Sci., **52**, pp1924-1933.

Pruppacher,H.R. and J.D.Klett (1997) Microphysics of clouds and precipitation, 2nd Ed., Kluwer Academic Publishers, Dordrecht.

Randall,D.A., J.Curry, P.Duynkerke, S.Krueger, M.Miller, M.Moncrieff, B.Ryan, D.Starr and W.Rossow. (2000) The second GEWEX Cloud System Study science and implementation plan. IGP0 Report 34.

Sassen,K. and S.Benson (2000) Ice nucleation in cirrus clouds: A model study of the momogeneous and heterogeneous modes. Geophys.Res.Lett., **27**, pp521-524.

Sassen,K. and G.C.Dodd (1988) Homogeneous nucleation rate for highly supercooled cirrus cloud droplets. J.Atmos.Sci., **45**, pp1357-1369.

Spice,A., D.W.Johnson, P.R.A.Brown, A.G.Darlison and C.P.R.Saunders (1999) Primary ice nucleation in orographic cirrus cloud: A numerical simulation of the microphysics. Q.J.R.Meteorol.Soc., **125**, pp1637-1667.

Starr,D.O'C. and G.C.Cox (1985) Cirrus clouds. Part 1: A cirrus cloud model. J.Atmos.Sci., **42**, pp2663-2681.

Tabazedeh,A., S.T.Martin and J.S.Lin (2000) The effect of particle size and nitric acid uptake on the homogeneous freezing of aqueous sulphuric acid particles. Geophys.Res.Lett., **27**, pp1111-1114.

Wilson,D.R. (2000) The impact of a physically based microphysical scheme on the climate simulation of the Meteorological Office Unified Model. Q.J.R.Meteorol.Soc., **126**, pp1281-1300.

Wilson,D.R. and S.P.Ballard (1999) A microphysically based precipitation scheme for the UK Meteorological Office Unified Model. Q.J.R.Meteorol.Soc., **125**, pp1607-1636.